ARTICLE
Journal of Cellular Biochemistry 114:2170–2187 (2013)

Journal of Cellular Biochemistry

The TERE1 Protein Interacts With Mitochondrial TBL2: Regulation of Trans-Membrane Potential, ROS/RNS and SXR Target Genes

William J. Fredericks,[1]* Terry McGarvey,[2] Huiyi Wang,[1] Yongmu Zheng,[1] Nathaniel J. Fredericks,[1] Hankun Yin,[1] Li-Ping Wang,[3] Wayland Hsiao,[4] Rob Lee,[5] Jayne S. Weiss,[6] Michael L. Nickerson,[7] Howard S. Kruth,[8] Frank J. RauscherIII,[9] and S. Bruce Malkowicz[1]

[1]*Division of Urology, Department of Surgery, University of Pennsylvania and Veterans Affairs Medical Center Philadelphia, Philadelphia, Pennsylvania, 19104*

[2]*Department of Anatomy, Kirksville Osteopathic Medical School, Kirksville, Missouri, 63501*

[3]*Department of Pathology and Laboratory Medicine, University of Pennsylvania Medical Center, Philadelphia, Pennsylvania, 19104*

[4]*Department of Urology, Weill Cornell Medical College, New York, New York, 10065*

[5]*Department of Otorhinolaryngology, University of Pennsylvania and Veterans Affairs Medical Center Philadelphia, Philadelphia, Pennsylvania, 19104*

[6]*Departments of Ophthalmology and Eye Center, Louisiana State University, New Orleans, Louisiana*

[7]*Cancer and Inflammation Program, National Cancer Institute, Frederick, Maryland, 21702-1201*

[8]*Section of Experimental Atherosclerosis, National Institutes of Health, Bethesda, Maryland*

[9]*The Wistar Institute, Philadelphia, Pennsylvania, 19104*

ABSTRACT

We originally discovered TERE1 as a potential tumor suppressor protein based upon reduced expression in bladder and prostate cancer specimens and growth inhibition of tumor cell lines/xenografts upon ectopic expression. Analysis of TERE1 (aka UBIAD1) has shown it is a prenyltransferase enzyme in the natural bio-synthetic pathways for both vitamin K-2 and COQ10 production and exhibits multiple subcellular localizations including mitochondria, endoplasmic reticulum, and golgi. Vitamin K-2 is involved in mitochondrial electron transport, SXR nuclear hormone receptor signaling and redox cycling: together these functions may form the basis for tumor suppressor function. To gain further insight into mechanisms of growth suppression and enzymatic regulation of TERE1 we isolated TERE1 associated proteins and identified the WD40 repeat, mitochondrial protein TBL2. We examined whether disease specific mutations in TERE1 affected interactions with TBL2 and the role of each protein in altering mitochondrial function, ROS/RNS production and SXR target gene regulation. Biochemical binding assays demonstrated a direct, high affinity interaction between TERE1 and TBL2 proteins; TERE1 was localized to both mitochondrial and non-mitochondrial membranes whereas TBL2 was predominantly mitochondrial; multiple independent single amino acid substitutions in TERE1 which cause a human hereditary corneal disease reduced binding to TBL2 strongly suggesting the relevance of this interaction. Ectopic TERE1 expression elevated mitochondrial trans-membrane potential, oxidative stress, NO production, and activated SXR targets. A TERE1-TBL2 complex likely functions in oxidative/nitrosative stress, lipid metabolism, and SXR signaling pathways in its role as a tumor suppressor. J. Cell. Biochem. 114: 2170–2187, 2013.

KEY WORDS: TERE1; TBL2; MITOCHONDRIA; LIPID METABOLISM; ROS; SXR TARGET GENES

Conflict of Interest Statement: The authors have declared that no conflicts of interest exist.

Grant sponsor: Veterans Affairs Merit Review; Grant sponsor: The Innisfree Foundation of Bryn Mawr, PA; Grant sponsor: The Castleman Family Fund.

*Correspondence to: Dr. William J. Fredericks, VA Medical Center Philadelphia, Research Building#21, Room A418, University and Woodland Ave, Philadelphia, PA 19104. E-mail: wjfredericks@verizon.net

Manuscript Received: 30 March 2013; Manuscript Accepted: 2 April 2013

Accepted manuscript online in Wiley Online Library (wileyonlinelibrary.com): 8 April 2013

DOI 10.1002/jcb.24567 • © 2013 Wiley Periodicals, Inc.

We originally reported the cloning of the TERE1 gene (aka UBIAD1) located on human chromosome 1p36, a site of frequent deletion in many cancer types including bladder. TERE1 was pursued because it was well expressed in bladder urothelium, however the mRNA was substantially reduced in muscle-invasive transitional cell carcinoma (TCC) of the bladder (22 out of 29 cases) and metastatic prostate cancer (14 out of 20 cases). A significant decrease in the TERE1 protein in both superficial and muscle invasive lesions of TCC compared to normal human urothelium was noted [McGarvey et al., 2001]. Ectopic expression of TERE1 in established cell models of bladder and prostate cancer resulted in dramatic inhibition of growth in vitro and tumorigenicity in vivo [McGarvey et al., 2001; McGarvey et al., 2003; Fredericks et al., 2011]. Together, these genetic and cell biology studies based findings suggested that TERE1 might be a 1p36 tumor suppressor gene.

Recent data from diverse sources/fields has painted an exciting albeit, incomplete picture of how TERE1 functions, most of which point to a role in cellular metabolism and energy homeostasis. Mutations in human TERE1 cause Schnyder's Corneal Dystrophy, (SCD), in which patients suffer from elevated corneal cholesterol and lipid deposition [Weiss et al., 2007; Nickerson et al., 2010]. In parallel, TERE1 was also re-discovered as a long sought after prenyltransferase enzyme in the vitamin K-2 biosynthetic pathway in which vitamin K-1 is converted to K-2 with K-3 as an intermediate [Nakagawa et al., 2010]. Vitamin K-2, also known as menaquinone, and vitamin K-3, also known as menadione, are redox-cycling and alkylating quinones known to inhibit the growth of tumor cells via activating oxidative stress responsive signaling cascades such as EGFR and AKT ([Nishikawa et al., 1999; Lamson and Plaza, 2003; Gilloteaux et al., 2010] and references therein). Vitamin K-2 is also a potent activator of SXR nuclear hormone receptor signaling which regulates transcription of multiple genes in pathways such as lipid metabolism and cholesterol efflux, a finding consistent with the SCD phenotype in human TERE1 mutants [Zhou et al., 2009a]. Exploring this hypothesis, we found that both ectopic manipulation of either TERE1 or TBL2 expression could modulate intracellular cholesterol levels [Fredericks et al., 2011]. TERE1 was also found to interact directly with HMGcoA reductase, HMGR, a principal regulator of cholesterol synthesis and sterol *O*-acyltransferase SOAT-1, involved in cholesterol storage [Nickerson et al., 2013]. SCD mutations have been shown to affect TERE1 interaction with APOE [McGarvey et al., 2005; Fredericks et al., 2011], and with HMGR [Nickerson et al., 2013]. The Drosophila homolog of TERE1/UBIAD1, heix, was demonstrated to play a role in vitamin K-2-mediated mitochondrial electron transport and ATP production, consistent with the long established role of menaquinone in anaerobic bacteria and mitochondria [Tielens et al., 2002; Nowicka and Kruk, 2010; Vos et al., 2012]. Recently the Xenopus homolog of TERE1/UBIAD1, barolo, was found to localize in golgi and function in the synthesis of non-mitochondrial COQ10 and the regulation of eNOS activity important for redox balance in endothelial cells [Mugoni et al., 2013]. Together these recent studies suggest that TERE1 may have different locations, substrates, and functions in different cell types and that TERE1 might integrate signals from multiple metabolic pathways.

We had expanded the functional analysis by discovering TERE1-interacting proteins and identified and validated an interaction with APOE, an established mediator of cholesterol and triglyceride uptake and recycling [McGarvey et al., 2005]. In this study we characterize the WD40 repeat protein TBL2 as a TERE1-interacting protein. The TBL2 gene is within a region of chromosome 7q11.23 deleted in Williams–Beuren syndrome and the protein has five WD40 domains [Perez Jurado et al., 1999]. TBL2 was implicated in TGFβ signaling via interaction with the ubiquitin ligase SMURF1 [Barrios-Rodiles et al., 2005], and has also been postulated as a disease gene in triglyceride disorders [Kathiresan et al., 2008]. Recently, TBL2 was found to interact with PDK1, implying a possible role in AKT signaling [Behrends et al., 2010]. Together these studies point to a role for TERE1 and TBL2 as potential modulators of cell stress and growth signaling, and lipid metabolism. How they work together is unknown. The nature of the interaction between these two proteins, and the functional consequences of that interaction are presented in this study.

Our data support a role for TERE1 and TBL2 in mitochondrial bioenergetics, oxidative and nitrosative stress, lipid metabolism, and SXR signaling. We discuss the hypothesis that compromise of TERE1 by reduced expression in invasive cancers and mutation in SCD, may represent a loss of redox sensing and SXR signaling that affects lipid metabolism and growth.

MATERIALS AND METHODS

CELL LINES AND ANTIBODIES

All cell lines were obtained from the American Type Culture Collection (Manassas, VA) and grown according to supplier's instructions. Polyclonal antibodies against specific peptide antigens of the human TERE1 (amino acids 31–45, 229–242, 301–314) and TBL2 (amino acids 111–129, 353–366, 413–426) proteins were prepared in rabbits or chickens at Invitrogen and were antigen affinity purified according to standard methods provided by Invitrogen. Goat anti-TERE1 antibodies were obtained from Santa Cruz. Rabbit anti-TBL2 (216–309) and hrp-mouse-anti-FLAG-M2 were obtained from Sigma. The protein A and protein G colloidal gold was from Electron Microscopy Sciences. The hrp-mouse-anti-XPRESS was from Invitrogen.

EXPRESSION VECTORS

The pcDNA3.1HisC-TERE1 plasmid was previously described [McGarvey et al., 2001, 2003, 2005]. The mammalian CMV expression plasmids pM12-NFLAG-TERE1, pM12-NFLAG-TBL2, and pM12-NFLAG-SMURF1 were obtained from GeneCopoeia. The pcDNA3.1-HisC TBL2 plasmid was derived by ligation of the *Eco*R1/*Xho*1 fragment of pTRG-TBL2 encoding the TBL2 full-length open reading frame into the *Eco*R1/*Xho*1 sites of the pcDNA3.1 HisC vector (Invitrogen), which was used as a negative control. Site-directed point and stop mutations in TERE1 and TBL2 were constructed using the Stratagene quickchange XL mutagenesis strategy with pM12-NFLAG-TERE1 and pM12-NFLAG-TBL2 plasmids as templates and appropriate mutagenic primers as specified by the manufacturer. The bacterial expression plasmids pB04-GST-TBL2, and GST-TERE1 plasmids were obtained from GeneCopoeia. The pGEX4T vector was from Pharmacia. All plasmids were sequenced to verify coding sequences, point and deletion mutations, reading frames, and were

amplified and purified by standard techniques. The Ad-TERE1, Ad-TBL2, and Ad-LACZ adenovirus plasmids were derived using Gateway LR recombination of the pAd/CMV/V5DEST vector with a pDONR221-TERE1, TBL2, or LACZ entry plasmid following recommendations from Invitrogen [Fredericks et al., 2011]. Infectious adenovirus was produced and amplified in HEK-293A cells following guidelines from Invitrogen and titered via an anti-hexon staining procedure from Clontech to $>4 \times 108$ IU/ml. Infections were in the presence of 6 μg/ml polybrene and monitored via AdGFP expression. Plasmids were quantitated by UV and Picogreen assay (Invitrogen) and evaluated on ETBr stained agarose gels.

INDIRECT IMMUNOFLUORESCENCE

Standard procedures for TERE1 and TBL2 immunofluorescence microscopy of J82 and T24 cell lines are detailed in Supplemental Methods. Cells were viewed under a fluorescence microscope (Nikon Eclipse TE2000) and digital images were captured with Image Pro plus V5 software. Negative controls were treated in the same way, except that the primary antibody, or one of the primary antibodies for double labeling, was omitted.

IMMUNO-ELECTRON MICROSCOPY

Cell pellets of J82 cells (uninfected, Ad-TERE1, Ad-TBL2 infected) were cryogenically frozen with an Abra HPM010 and freeze substituted in 0.2% gluteraldehyde, 0.1% uranyl acetate in anhydrous acetone in a Lieca AFSII at −90°C for 2 days. Freeze substitution solutions were warmed to −50°C over 12 h and washed in acetone and then replaced with graded exchanges of HM20 for 48 h, followed by UV polymerization at −50°C for 48 h. Thin sections of 70 nm thickness were labeled with Goat anti-TERE1 SC47474 at a 1/10 dilution in 5% BSA, 0.1% cold water fish gelatin, 0.1% Tween-20 in PBS. Secondary detection was performed with protein-G conjugated to 15 nm gold. The TBL2 antibody was the Sigma HPA007477 and the secondary detection was carried out with protein-A 6 nm Au conjugate. Electron microscopy imaging was performed on a Tecnai-12 at 80 KeV equipped with a Gatan US1000 4 mp camera. Montage images were generated in SerialEM and stitched into montages with Blendmont in the IMOD package.

NUCLEOFECTION

Nucleofection was performed with the Nucleofector II system according to the manufacturer's protocol (Amaxa/Lonza Cologne, Germany). Briefly, cells were passaged 3 days before nucleofection and grown to 70% confluency. Cells were harvested by trypsinization and 3×10^6 cells were mixed with 100 μl of nucleofector solution and 3 μg plasmid DNA. Samples were transferred into cuvettes and nucleofected using program Q001 and solution S for HEK-293 cells. Cells were re-suspended in growth medium and allowed to grow for 1–3 days. HEK-293 cells exhibited a >95% transfection efficiency and a >90% viability via trypan blue staining. Expression plasmids were controlled with parallel nucleofections of CMV empty vector.

CELL EXTRACTS, CO-IMMUNOPRECIPITATION, AND GST ASSOCIATION

Cell lines plated in 10 cm dishes had been transfected via Amaxa nucleofection or transduced with Ad-LACZ, Ad-TERE1, or Ad-TBL2 adenovirus, and harvested 36–72 h later by washing in ice cold PBS with protease inhibitors, and scraping to freeze cell pellets. Whole cell extracts were prepared and analyzed by methods detailed in Supplemental procedures. The procedures for co-immunoprecipitation and GST association assays are detailed in the Supplemental Methods.

OXIDATIVE AND NITROSATIVE STRESS ASSAYS

Oxidative stress measurements were conducted using cell imaging of dihydrorhodamine 123 and CellROX deep red fluorogenic probes (Molecular Probes/Invitrogen). Dihydrorhodamine 123 reacts with either hydrogen peroxide (in presence of peroxidase, cytochrome *c*, or Fe^{2+}) or with peroxynitrate (formed when nitric oxide reacts with superoxide). Once Dihydrorhodamine 123 is oxidized to rhodamine 123, it localizes to mitochondria. CellROX Deep Red oxidation is specific for ROS but not RNS. J82 cells were plated in 96-well optically clear plates (Costar 3720) and infected for 48–72 h with Ad-LACZ, Ad-TERE1, or Ad-TBL2. Following infection, cells were washed in warm M199 and then incubated in the dark with 5 μM diydrorhodamine 123 (Invitrogen D-23806) for 15 min at 37°C. After subsequent washing, cells were visualized using a laser scanning confocal microscope (Olympus Fluoview FV1000; 488 nm Ar laser excitation/525 nm emission; 10×, 0.3NA objective). Replicate J82 cultures were washed in warm M199 medium and then incubated with 5 μM CellROX deep red reagent for 30 min at 37°C, washed three times with PBS, and fixed for 15 min with 3.7% formaldehyde. Vitamins K-2, and K-3 (Sigma Chemical Co.) were applied to cell cultures for 1 h at 30 μM prior to dye loading as controls. Confocal imaging of CellROX oxidation was performed using 635 nm diode laser excitation and 680 nm emission. Cellular fluorescence intensities were quantified after off-cell background subtraction. Preliminary experiments determined that unlabeled cells exhibited negligible autofluorescence at these settings.

CASPASE 3/7 ASSAYS

Caspase 3/7 assays used the Promega Caspase-Glo luciferase assays as specified by manufacturer. J82 cells were plated in 96-well luminometry plates for cell culture and quadruplicate wells infected for 60 h with Ad-LACZ, Ad-TERE1, or Ad-miRNA TERE1 [Fredericks et al., 2011].

CELLULAR NO/RNS PRODUCTION

Cellular NO/RNS production was measured using the fluorescent probe 4-amino-5-methylamino-2′,7′-difluorofluescein diacetate, DAF-FM-DA (Molecular Probes/Invitrogen; D-23844); DAF-FM reacts with NO and RNS to form a fluorescent benzotriazole. Confocal DAF-FM imaging was performed using the 488 nM laser line of the same confocal system described above (525 nm emission). J82 cells were plated in cover glass bottom culture dishes (MatTek P35G-1.0-14C) and were infected for 48–72 h with Ad-LACZ, or Ad-TERE1. After washing three times in warm Hank's Balanced Salt Solution (HBSS: (in mM) 137 NaCl, 5 KCl, 0.4 KH_2PO_4, 0.3 Na_2HPO_4, 5.5 glucose, 1.8 $CaCl_2$, 1.5 $MgCl_2$, 10 HEPES, pH 7.3), they were loaded with DAF-FM by incubation in DPBS containing 5 μM DAF-FM DA and 5 μM carboxy PTIO (Cayman Chemicals), a cell permeant NO scavenger to prevent DAF-FM from reacting with any RNS produced

during dye loading. After 45 min loading at room temperature in the dark, cultures were washed four times with warm HBSS to remove unloaded DAF-FM DA and cPTIO, followed by ~10 min to allow for loaded dye retention before imaging was performed. Care was taken to follow the loading protocol strictly to normalize dye loading between samples. Images were captured at 10-s intervals (scan speed 12 μs/pixel). Additionally, microscope/software settings (laser power, offset, gain, PMT voltage, confocal aperture, etc.) were identical for every experiment within each dye. No gain, offset or gamma alterations were used. Baseline DAF FM fluorescence was determined by averaging the first 20 frames of each experiment. NO production was initiated by addition of modified Hank′s Balanced Salt solution (HBSS; pH 7.4) containing 1× minimal essential medium (MEM) amino acids (Gibco) to provide a source of arginine (~0.6 mM) for NO production and measured for 10 min. Menaquinone 30 μM was added to one set of Ad-LACZ or Ad-TERE1-infected J82 cells for 1 h prior to imaging as well as during imaging to assess immediate responses. Normalization of DAF FM fluorescence changes was made after subtraction of off-cell background fluorescence.

MITOCHONDRIAL TRANSMEMBRANE POTENTIAL MEASUREMENTS

JC-1 (5,5′,6,6′-tetrachloro-1,1′,3,3′-tetra-ethylbenzimidazolocarbocyanine iodide, Molecular Probes/Invitrogen) was used to visualize changes in mitochondrial transmembrane potential of J82 cells after 72 h transduction with Ad-LACZ, Ad-TERE1, Ad-TBL2, or 1 h treatment with menaquinone (30 μM). JC-1 exhibits a potential dependent accumulation in mitochondria, shifting in emission from green to red as the potential increases and the JC-1 undergoes concentration dependent aggregation. Briefly, treated cells were washed with PBS, and labeled with 2 μM JC1 via incubation for 15 min at 37°C in a CO_2 incubator protected from light. Carbonyl cyanide m-chlorophenylhydrazone (CCCP) (50 nM), a protonophore, was used as a mitochondrial uncoupler for 2 min at 37°C prior to visualization to confirm that the JC-1 response was sensitive membrane potential depolarization as evidenced by green staining indicative of monomeric dye. After incubation, the cells were washed again with warm PBS to remove excess tracer and were then analyzed by confocal microscopy using standard filters for Alexa Fluor 488 (488 nm excitation, 529 nm emission) and R-phycoerythrin (549 excitation, 590 emission) based on the excitation and emission peaks of monomeric and aggregate forms of JC-1, respectively.

CHOLESTEROL ASSAY

The cholesterol content of J82 cell lysates harvested after 72 h of transduction with Ad-LACZ, Ad-TERE1, Ad-TBL2, or treatment with vitamin K-1 (30 μM), K-2 (30 μM), K-3 (10 μM) was detected using an Amplex Red Cholesterol Assay kit relative to a dilution series of cholesterol standards as specified (Invitrogen). Lysates were prepared as previously described [Fredericks et al., 2011].

RNA ISOLATION, REVERSE TRANSCRIPTION AND FLUIDIGM RT-PCR TAQMAN EXPRESSION ASSAYS

J82 cells were grown to 80% confluency, transduced with Ad-LACZ, Ad-TERE1, Ad-TBL2, and ~5 × 10e6 cells were lysed in 2 ml Trizol after 72 h. Total RNA was isolated from TRIzol cell lysates (Invitrogen, Carlsbad, CA), using the Ambion Pure-Link RNA Mini kit according to procedures specified by the manufacturer (Catalog 12183-081A). RNA quantity was determined using a Nanodrop ND-1000 spectrophotometer (Thermo Scientific, Waltham, MA) and quality was assessed at the UPENN Molecular Profiling Facility using an Agilent 2100 Bioanalyzer (Agilent Technologies, Santa Clara, CA). The cDNA synthesis, specific target pre-amplification, and Fluidigm RTPCR Taqman expression assays were performed using procedures recommended by ABI Biosciences and Fluidigm and are detailed in the Supplemental Methods. Data was analyzed using the BioMark Gene Expression Data Analysis software to obtain $\Delta\Delta C_t$ values and expressed as a ratio to the Ad-vector control to determine the fold change in gene expression. The Taqman probes were purchased from Applied Biosystems/Invitrogen and are listed in the Supplemental Methods.

RESULTS

FEATURES OF TERE1 (UBIAD1) AND TBL2 PROTEINS

A ten α-helical trans-membrane domain diagram for the 338 amino acid TERE1 protein is shown in Figure 1A [Nickerson et al., 2010; Fredericks et al., 2011]. A pTARGET analysis predicted that both TERE1 and TBL2 would exhibit a mitochondrial sub-cellular localization [Guda and Subramaniam, 2005]. Frequent positively charged lysine and arginine residues suggest that the NH2-terminus of both TERE1 and TBL2 proteins may insert across the outer mitochondrial membrane. As depicted, the mutations (in red) associated with SCD occur in residues on one side of the membrane, either in aqueous loops or transmembrane helices close to one bilayer surface [Weiss et al., 2007]. These loops may constitute a binding interface for interacting proteins, APOE and TBL2 [Fredericks et al., 2011], or the sterol sensing 5TM box of HMGR and sterol *O*-acyltransferase SOAT-1 [Nickerson et al., 2013]. Also featured is a well-conserved CRAC motif (L/V(X_{1-5})Y(X_{1-5})R/K) similar to several cholesterol transporter proteins [Jamin et al., 2005], and an adjacent FARM motif DDXXXXD (farnesyl binding aspartate-rich motif). This region has also been referred to as a putative ligand/polyprenyldiphosphate binding site [Weiss et al., 2007]. The approximate polyclonal antibody binding sites used in this study, and the sites of engineered stop mutations at Y174 and E242, which approximate the positions of two reported splice variants, G179 and M237, are also shown. The presence of a heme regulatory motif (30-XCPXX-34) and oxido-reductase motif (145-CXXC-148), not shown, suggests that TERE1 activity may be affected by cellular redox state [Weiss et al., 2007]. Overall the interacting proteins APOE, HMGR, and SOAT-1 support a localization in ER and golgi and a role in cholesterol synthesis and regulation; however, this report supports additional interaction with TBL2 in mitochondria, and modulation of SXR targets consistent with its role in synthesis of vitamin K-2.

A schematic of the 448 amino acid TBL2 protein (Fig. 1B), shows a single NH2-terminal trans-membrane domain, TMB, five WD40, β-transducin repeat domains, and a nuclear localization signal, NLS. Included are the binding sites for the polyclonal antibodies and the point mutations used to create deletion proteins (TBL2-Y174 STOP and -E311 STOP) to map protein interactions with TERE1. The two rough models of TBL2 structure emphasize its single trans-membrane

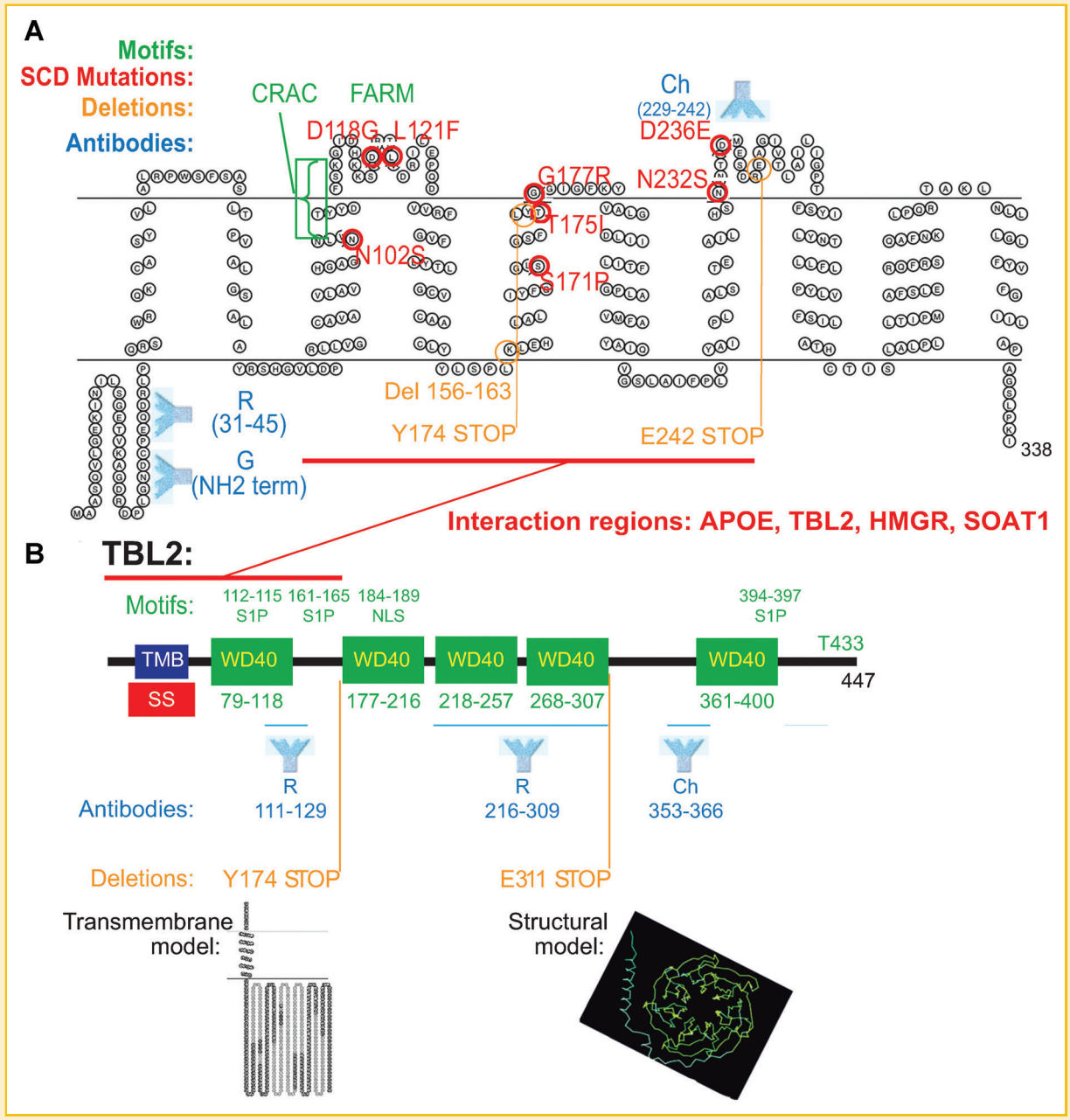

Fig. 1. Diagrams of TERE1 and TBL2: 1A. Trans-membrane model of the TERE1 protein depicting sites of SCD point mutations (red), the conserved CRAC and FARM motifs (green). 1B. Sketch of the TBL2 protein showing a single trans-membrane domain, TMB, five WD40 domains, a putative nuclear localization sequence, NLS, and putative S1P cleavage sites. For both TERE1 and TBL2 the sites of engineered stop mutations causing deletions (orange), the antigen regions for polyclonal antibodies are shown (blue), and the regions of protein interactions are noted (red).

domain and the propeller structure of the WD40 domain repeats (http://modbase.compbio.ucsf.edu). Also shown is a site of phosphorylation at T433 by ATM/ATR in response to genomic damage [Matsuoka et al., 2007], and three putative SKI-1/S1P protease cleavage sites we have recognized in the TBL2 sequence.

TERE1:TBL2 TWO-HYBRID INTERACTION

A two-hybrid analysis had identified APOE as a putative TERE1 (UBIAD1)-interacting protein [McGarvey et al., 2005] and also recovered three independent TBL2 clones, however the interaction had not been validated. In this study we used the stringent reporter strain of Bacteriomatch System II to validate the two-hybrid interaction of TERE1 with TBL2. Table SI in Supplemental Results shows the number of colonies after co-transformation of 50 ng of the pBT-TERE1 bait and pTRG-TBL2 target plasmids, and growth at 30°C for 30–40 h. The negative controls show no colonies: pBT plus pTRG (vectors alone), pBT-TERE1 (bait alone) plus pTRG vector, pBT vector + pTRG-TBL2 (target alone); hence, no self-activation of

reporter by TERE1or by TBL2 alone. The positive control shows an abundance of colonies, pBT-LGF2 + pTRG-gal 11p. The test of the interaction of pBT-TERE1 + pTRG-TBL2 shows positive surviving colonies that confirm the two-hybrid TBL2 interaction.

TERE1 AND TBL2 ANTIBODIES

We developed polyclonal antibodies against specific peptide antigens of the human TERE1 (amino acids 31–45, 229–242) and TBL2 (amino acids 111–129, 353–366) protein sequences. Figure 2 shows immunoblot examples from cell lysates of HEK-293 cells transfected with CMV FLAG or XPRESS-tagged TERE1 or TBL2 expression plasmids and empty CMV vector and probed with different affinity purified antibodies (anti-TERE1, top, and anti-TBL2, bottom). Beneath each panel, the amino acid residues of the antigen and the species in which the antibody was raised are indicated. TERE1 is resolved at its predicted size of ~37 kDa and TBL2 at its predicted size of ~49 kDa along with a more slowly migrating potentially modified form. Detection of 3XFLAG or XPRESS epitope tagged TERE1 and TBL2 is shown for comparison with endogenous.

TERE1 AND TBL2 SUB-FRACTIONATION

Sub-cellular fractions were prepared from the J82 transitional cell carcinoma cell line and equal amounts of endogenous proteins were analyzed by immunoblots with goat anti-TERE1 (NH2), and rabbit anti-TBL2 (216–309). Both proteins are enriched in the membranous, organellar fractions (Supplemental Fig. 1). Immunoreactivity for TERE1 in the nuclear fraction may be due to co-pelleting of trapped membranous fragments, based on a lack of nuclear staining in immuno-electron micrographs. For TBL2, however, we did observe infrequent and minor nuclear immunoreactivity, by immuno-fluoresence (Supplemental Fig. 2) and -electron microscopy (data not shown). A 20–30 kDa-shifted form of TERE1 was observed exclusively in the cytoplasmic fractions (Supplemental Fig. 1A), suggesting distinct subcellular pools or possible modifications, consistent with reports of different subcellular locations (The possibility of a minor cross-reaction can not be ruled out). Additional larger TBL2 forms are also observed: one, shifted by 20 kDa is seen in the cytoplasmic fraction, and another form shifted by 10 kDa in the membranous and nuclear fraction. Immunoblot analysis of a mitochondrial fraction isolated from human liver by Mitosciences, also shows co-expression of TERE1 and TBL2.

CO-IMMUNOPRECIPITATION OF TERE1 AND TBL2

We confirmed the TERE1 and TBL2 interaction by co-immunoprecipitation (Fig. 3) from cell lysates after transfection of expression plasmids encoding differently tagged TERE1 and TBL2 proteins (XPRESS or Flag). The lanes depicting the co-immunoprecipitation are indicated as CO-IP, for three different precipitating antibodies: mouse anti-XPRESS, rabbit anti-TBL2 (111–129), or goat anti-TERE1-N, and detected with hrp mouse anti-Flag M2. The FLAG-TERE1 and FLAG-TBL2 lysates were loaded in the same lane as a straight lysate (SL) positive control. Adjacent lanes with arrows show replicate immunoprecipitations. For both TERE1 and for TBL2, the fact that different antibodies from different species and to different regions of the protein detect the same protein in an IP-western validates their specificities. The co-expression and co-precipitation of TERE1 and TBL2 prompted us to examine their sub-cellular location.

TERE1 AND TBL2 SUB-CELLULAR LOCALIZATION

We used immunoflourescence microscopy to evaluate the endogenous subcellular localization of TERE1 and TBL2 in the J82 (Fig. 4) and T24 bladder cancer cell lines. A similar perinuclear/organellar pattern was observed for five anti-TERE1 and two rabbit anti-TBL2 antibodies (Supplemental Fig. 2). TERE1 did not appear to be localized to plasma membrane. We identified mitochondrial co-localization of TBL2 and TERE1 relative to the pattern obtained with anti-OXPHOS IV protein as a mitochondrial marker in the J82 (Fig. 4) and T24 bladder cancer cell lines (not shown). The TERE1, TBL2, and mitochondrial co-localization is most evident as a perinuclear distribution (yellow). However, TERE1 also shows significant non-mitochondrial areas of expression (green) consistent with ER, golgi, or other membranous compartments. TBL2 appears to be primarily coincident with mitochondria (yellow overlap), except for an infrequent nuclear staining (Supplemental Fig. 2).

TERE1 AND TBL2 IMMUNOELECTRON MICROSCOPY

To obtain a more precise subcellular localization we conducted immune-electron microscopy using the goat-anti TERE1 and rabbit anti-TBL2 affinity purified antibodies to label the control parental J82 cells, and J82 populations infected with Ad-TERE1, and Ad-TBL2 (Fig. 5). For the endogenous, Ad-TERE1, and Ad-TBL2 cell populations, the detection of anti-TERE1 staining (with a protein-G 15 nm colloidal gold secondary), reveals TERE1 in multiple membranous compartments, including mitochondria and non-mitochondrial vesicles. There were no obvious golgi stacks observed in these cells so without additional secondary markers the identity of the non-mitochondrial membranes can not be discerned. Using a protein-A 6 nm colloidal gold detection for anti-TBL2, we found the TBL2 staining pattern to be almost exclusively in inner mitochondrial membranes, with very little non-mitochondrial staining except infrequent nuclear clusters (not shown). Unlike immunoflourescence microscopy which uses detergents to improve access of antibodies to membrane proteins, the plastic embedding and sectioning process involved in immuno-electron microscopy allows detection only of those epitopes exposed in a particular section, hence probably under-represents the actual distribution. All together these data demonstrate that TERE1 and TBL2 co-localize and may interact in mitochondrial membranes, although TERE1 has additional non-mitochondrial sub-cellular organellar/membranous pools, consistent with reports of expression in ER and golgi.

TERE1 INTERACTION MAPPING

We used a GST association strategy to map the regions of TERE1 that could interact with TBL2. Flag-tagged test protein lysates (TERE1, TBL2, and SMURF1) were tested for binding to purified GST fusion protein baits (GST-vector, -TBL2, and -TERE1). Figure 6A shows the expression of baits and test lysates. Our deletion analysis (Supplemental Fig. 3) found that the middle third of TERE1 (E242 STOP) binds to the NH2-terminal third of TBL2 (Y174 STOP) and also shows that the TERE1/TBL2 binding assay works when configured in reverse: A GST-TERE1 bait protein can pull down Flag-TBL2 full

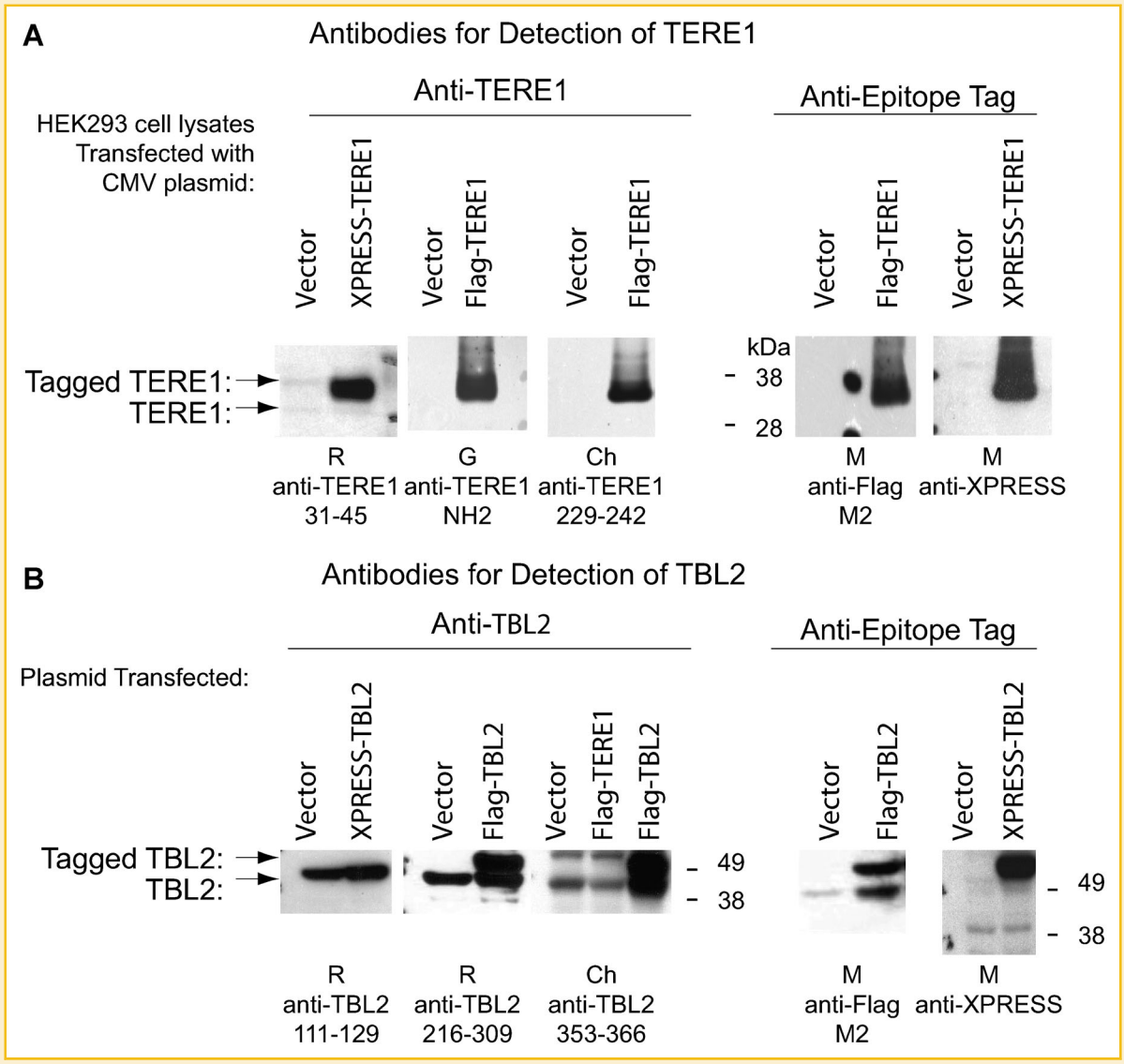

Fig. 2. TERE1 and TBL2 expression: Polyclonal antibodies to TERE1 (1A) and TBL2 (1B) were used to detect exogenous expression in HEK 293 cell lysates after transfection with CMV FLAG or XPRESS–tagged TERE1 or TBL2 plasmid or empty CMV vector. TERE1 is resolved at expected size of ~37 kDa and TBL2 at ~49 kDa. Mr refers to relative migration of standard marker proteins in kDa. Numbers refer to amino cid locations of antigenic regions for polyclonal antibodies.

length test proteins (and TBL2 deletions Y174-STOP and E311-STOP). To provide some further validation of our binding assay, we also confirmed a previously reported SMURF1/TBL2 interaction [Barrios-Rodiles et al., 2005] (Supplemental Fig. 4), which shows that both TERE1 and SMURF1 can bind TBL2.

NATURAL MUTATIONS IN TERE1

Next, we tested whether natural point mutations in TERE1 associated with SCD [Weiss et al., 2007] would affect binding to TBL2 (Fig. 6B). We found that the binding of mutants D118G, L121F, T175I, G177R, and N232S was reduced compared to wild type. This opens the possibility that an impaired protein interaction with TBL2 may contribute to the phenotype of SCD. A small deletion directed to the opposite side of the membrane, to TERE1 (156–163) or a K156R mutation, had no effect.

MITOCHONDRIAL TRANSMEMBRANE POTENTIAL

Based on the co-localization of TERE1 and TBL2 in mitochondria, the role of TERE1 in menaquinone synthesis [Nakagawa et al., 2010], and the established properties of menaquinone in electron transfer in anaerobic bacteria [Nowicka and Kruk, 2010], anaerobic mitochondria [Tielens et al., 2002], and mitochondria of Drospohila [Bhalerao and Clandinin, 2012; Vos et al., 2012], we examined whether ectopic TERE1 or TBL2 would affect the mitochondrial transmembrane potential of J82 bladder cancer cells using the voltage sensitive dye JC-1 following guidelines from Invitrogen. Figure 7 depicts confocal microscopic fluorescence images of J82 cells that had been infected with Ad-LACZ, Ad-TERE1, or Ad-TBL2 or pre-treated with vitamin K-2 (30 μM) or CCCP and loaded with the dye JC-1. The JC-1 dye exhibits an accumulation in mitochondria and a shift in emission from green to red as JC-1 undergoes a concentration-dependent

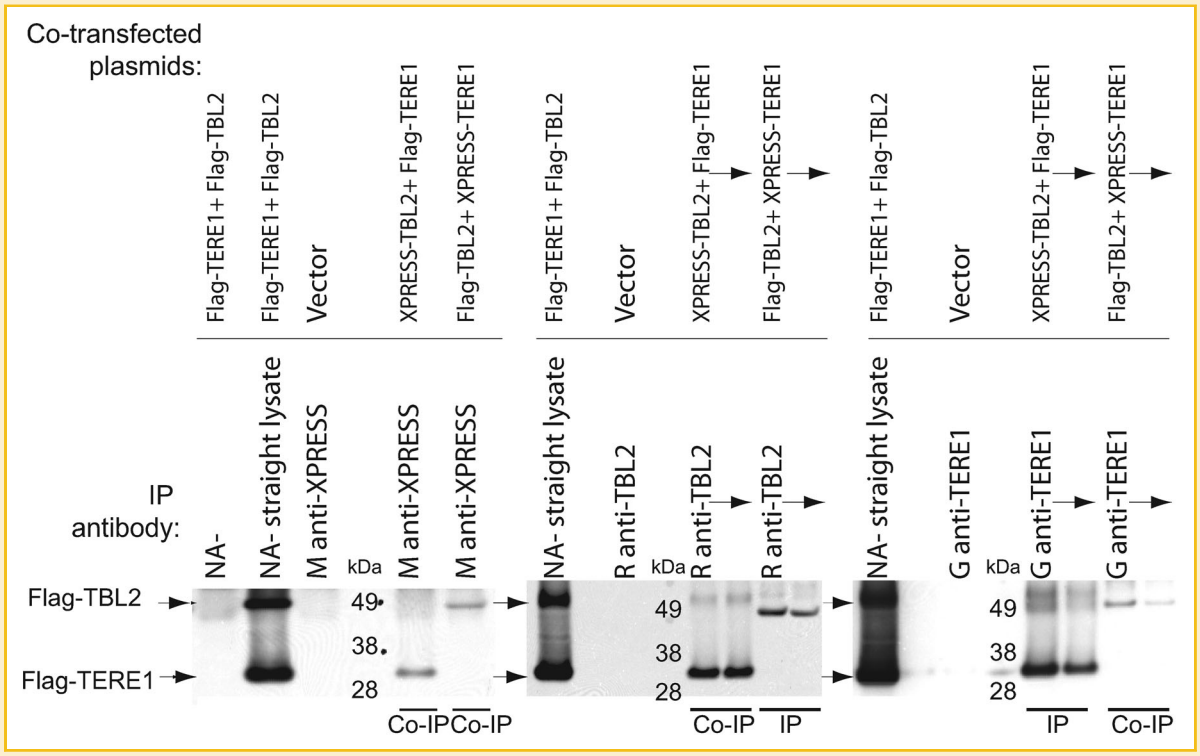

Fig. 3. Co-immunoprecipitation of TERE1 and TBL2. Co-immunoprecipitation of exogenous epitope-tagged (Flag or Xpress) TERE1 and TBL2 by IP-Western. IP refers to immunoprecipitation and Co-IP, Co-immunoprecipitation. Positive control is a mixture of Flag-TERE1 and Flag TBL2 lysates. Blots were probed with hrp-anti Flag M2 antibody.

aggregation with increasing transmembrane potential. The control Ad-LACZ cells show a similar degree of green and red staining cells, reflecting both monomeric and aggregated JC-1, respectively, and serve as a basal control representation of transmembrane potentials in a cell population. However, the Ad-TERE1 and AD-TBL2 infected cells show an obviously increased proportion of cells with more intense red staining, indicative of aggregated JC-1 due to an increased transmembrane potential. A similar increase in red staining is observed after treatment with menaquinone (K-2), the product of TERE1 prenyltransferase activity. To confirm that the JC-1 response of J82 cells was sensitive to membrane potential depolarization, carbonyl cyanide m-chlorophenylhydrazone (CCCP; 50 nM), a protonophore, was used as a mitochondrial uncoupler to depolarize the mitochondria causing green, monomeric, JC-1 staining in almost all cells. Since mitochondrial transmembrane potential drives ATP production, it is clear that TERE1 and TBL2 dosage may have effects on mitochondrial energy production.

TERE1-MEDIATED OXIDATIVE AND NITROSATIVE STRESS

Based on the propensity of menaquinone to undergo redox-cycling and generate reactive oxygen species, ROS [Klaus et al., 2010], and the activity of TERE1 in menaquinone synthesis [Nakagawa et al., 2010], we sought to evaluate whether TERE1 or TBL2 expression might affect the cellular levels of oxidative stress. We conducted imaging of J82 cells that had been loaded with CellROX deep red or dihydrorhodamine 123 fluorogenic probes after infection with Ad-LACZ, Ad-TERE1, or Ad-TBL2, or pre-incubation with menaquinone (K-2) or menadione (K-3). Figure 8, left side (red), shows that compared to the control Ad-LACZ infected cells (719 flourescence units, FUs), the Ad-TERE1 (1,067 FUs) and AD-TBL2 (1,167 FUs) infected J82 cells show an increase of over 40% in CellROX Deep Red staining intensity, and an over threefold increase (2,729 FUs) after treatment with 30 μM menadione for 1 h. We also found that J82 cells transduced with Ad-MiTERE1 to knockdown TERE1 levels also showed a 44% increase in CellROX oxidation (1,033 FUs). CellROX Deep Red oxidation is specific for ROS but not reactive nitrogen species, RNS. Dihydrorhodamine 123 reacts with either hydrogen peroxide or with peroxynitrate, is oxidized to rhodamine 123, and then localizes to mitochondria. Figure 8, right side (green), shows that compared to the Ad-LACZ J82 cells (1,789 FUs), the Ad-TERE1 over-expressing cells (2,376 FUs) show an increase in green rhodamine 123 of over 30%, and both the K-2-treated (2,845 FUs) and K-3-treated (2,761 FUs) cells show increases of over 50%. Additional experiments (Supplemental Fig. 5) found that ectopic TERE1 was associated with a twofold increase in caspase 3/7 activity, consistent with elevated ROS and known toxicity of menaquinone. In summary ectopic expression of TERE1, and TBL2 or pre-incubation with K-2 or K-3 can elevate ROS, which is consistent with the observed increased transmembrane potential and electron transport ability of menaquinone since the electron transport chain is an abundant source of mitochondrial superoxide radicals [Cardoso et al., 2012].

NITRIC OXIDE PRODUCTION

We evaluated the potential for ectopic TERE1 or menaquinone to elevate nitric oxide, NO, based on previous reports that K-2 could induce iNOS [Sano et al., 1999] and that SXR activation could

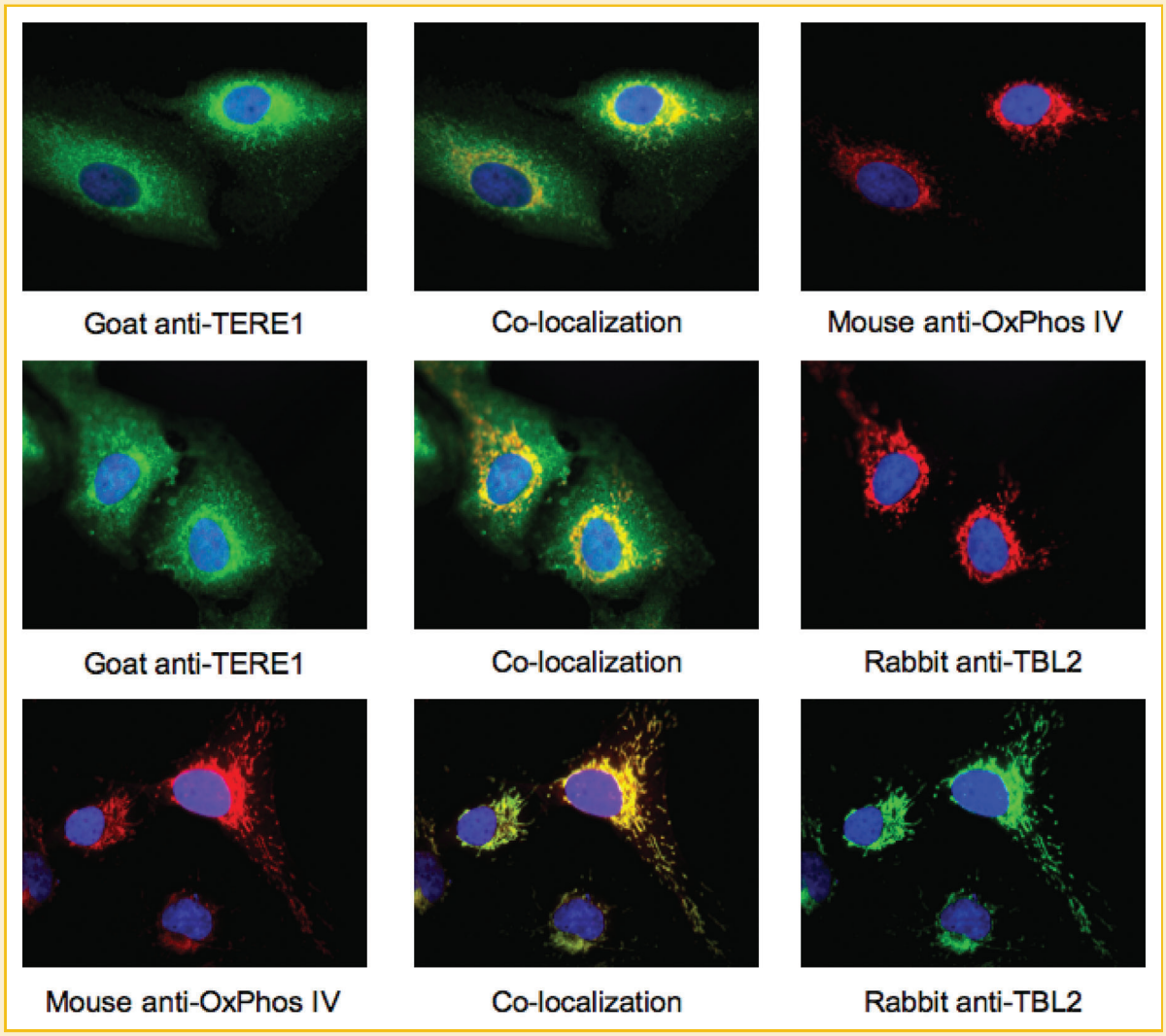

Fig. 4. Endogenous TERE1 and TBL2 co-localize with mitochondria in the J82 human bladder cancer cell line. Goat anti-TERE1 (N), Alexa fluor 594 labeled Mouse anti-OXPHOS IV (Invitrogen), and Rabbit anti-TBL2 (111–129) antibodies were used for immuno-fluorescence localization as described in methods. Secondary antibodies were: top, Alexa fluor 488 DAG, middle, Alexa fluor 488 DAG, and Alexa fluor 595 DAR, bottom, Alexa fluor 488 DAR are detailed in Materials and Methods Section (D for donkey, G for goat, R for rabbit.).

increase NO production [Verma et al., 2009]. We conducted live cell imaging of J82 cells that had been loaded with the DAF-FM-DA fluorogenic probe after infection with Ad-LACZ or Ad-TERE1 or pre-incubation with menaquinone (K-2). DAF FM reacts with NO and RNS to form a fluorescent benzotriazole. The graph in Figure 9 (left panel) compares the increases in fluorescence of J82 Ad-LACZ and Ad-TERE1 pre-infected cells, as an indicator of NO production. It is clear that the basal NO level of the J82 TERE1 cells is elevated by ~40% over the J82 Ad-LACZ population. Upon addition of vitamin K-2 (30 μM) to the cells, a slight increase in the rate of NO production is noted for the J82 Ad-LACZ cells, but little immediate change is observed in the J82 TERE1 cells. In the right panel, the cells were pre-incubated with 30 μM K-2 for an hour prior to loading with DAF FM DA. There is an obvious elevation of the initial baseline NO with the J82 Ad-LACZ cells, but little change was seen in the initial basal level of the J82 TERE1 cells. However, both the J82 Ad-LACZ and J82 TERE1 cells show a twofold increased rate of NO production upon further addition of K-2. The fact that increases could be observed within minutes of K-2 dosing suggests direct chemical mechanisms are likely involved. These results demonstrate that both ectopic TERE1 and K-2 can elevate NO, consistent with expectations of menaquinone ROS inducing properties and the elevated mitochondrial transmembrane potential though further study will be needed to clarify the exact subcellular sources.

TERE1, TBL2, AND K-2-INDUCED CHANGES IN CELLULAR CHOLESTEROL

We have previously demonstrated that ectopic expression of TERE1 or TBL2 can reduce cellular cholesterol levels in bladder cancer cell lines [Fredericks et al., 2011]. Given that TERE1 is involved in vitamin K-2 synthesis (from K-1, K-2, or K-3 Nakagawa), we tested whether pre-incubation with vitamin K derivatives would also reduce cellular

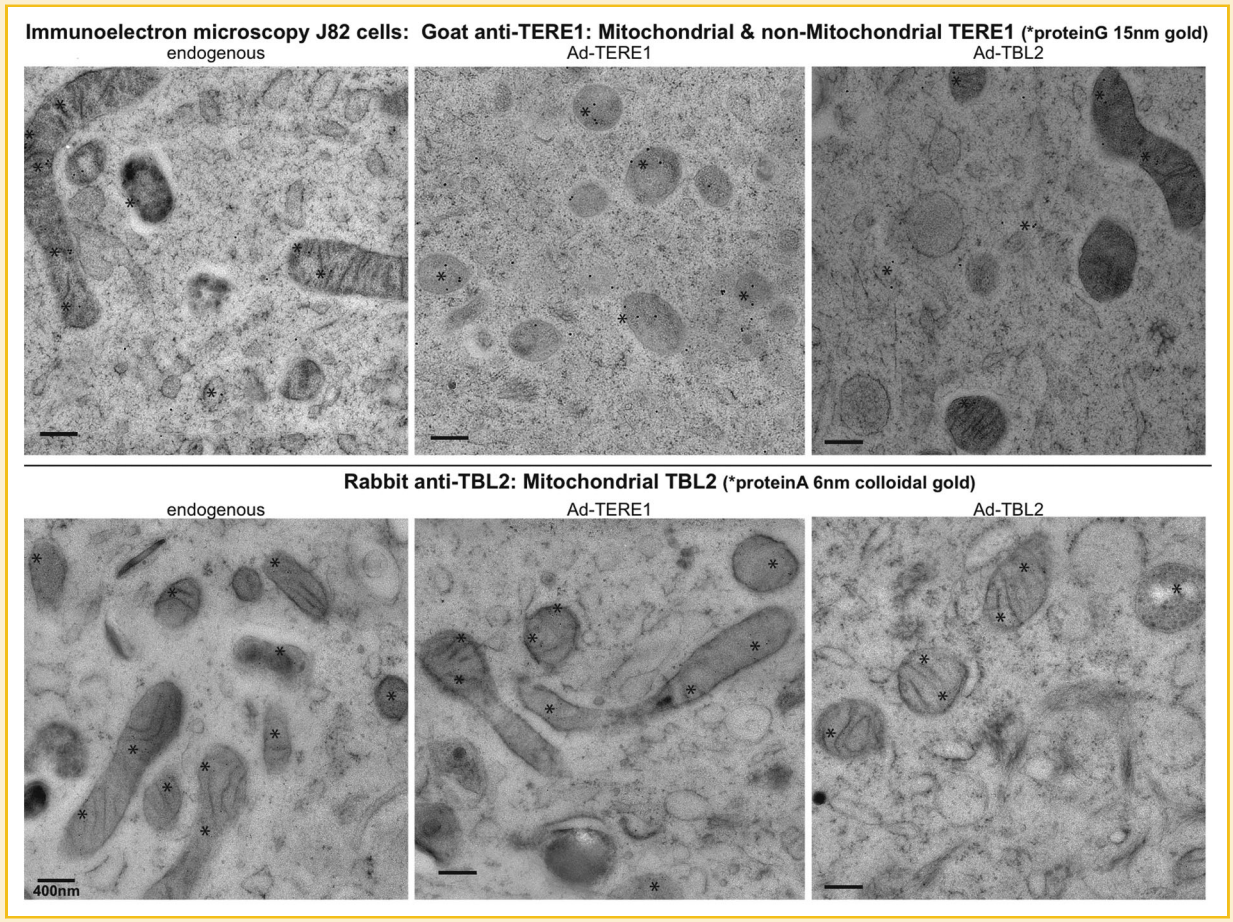

Fig. 5. Immuno-electron microscopic localization: TERE1 in mitochondria and non-mitochondrial vesicles and TBL2 in mitochondria. Top panels depict TERE1 detection with protein G 15 nm colloidal gold in endogenous J82 cells, J82 cells transduced with Ad-TERE1, and J82 cells transduced with Ad-TBL2. Bottom panels depict TBL2 detection with protein A 6 nm colloidal gold in mitochondria of endogenous J82 cells, J82 cells transduced with Ad-TERE1, and J82 cells transduced with Ad-TBL2.

cholesterol levels. Supplemental Figure 6 confirms that ectopic TERE1 and TBL2 reduce cell cholesterol by 20–30% and shows that a 72 h treatment of J82 cells with vitamin K-1 (30 μM), K-2 (30 μM), or K-3 (10 μM) can also reduce cellular cholesterol by at least 50%. This is consistent with a mechanism of K-2 mediated SXR activation of cholesterol efflux [Shearer and Newman, 2008; Zhou et al., 2009b].

TERE1, TBL2, AND K-2-INDUCED CHANGES IN SXR TARGET GENE EXPRESSION

Next we used Fluidigm RT-PCR Taqman expression assays [Spurgeon et al., 2008] to explore whether ectopic TERE1, TBL2 or treatment of J82 cells with vitamin K-2 (30 μM) would induce changes in expression of known SXR target genes. SXR has established roles in regulation of endobiotic homeostasis, energy metabolism, and Phase I and II enzymes and transporters involved in drug metabolism and clearance [Zhou et al., 2009b; Ihunnah et al., 2011]. We selected established target genes of SXR, and several genes involved in cholesterol synthesis and catabolism (refer to the list of Taqman expression assays in Supplemental Methods). We also evaluated selected LXR target genes because SXR is known to cross regulate LXR target genes [Zhou et al., 2009b]. The Venn diagram in Figure 10 summarizes our findings and depicts the fold-change in gene expression after three different induction treatments: TERE1 over-expression (red), vitamin K-2 treatment (30 μM overnight) (orange), and TBL2 over-expression (blue) relative to AD-LACZ or parental cell control and normalized as described in Materials and Methods Section. We have grouped the changes as to whether they are in common to all three induction treatments, or pairs of treatments, or only to individual induction treatments. Only genes that changed are depicted. The main point is that, as predicted, a number of SXR target genes involved in cholesterol and fatty acid regulation are induced, which is consistent with the hypothesis of TERE1-mediated vitamin K-2 activation of SXR nuclear receptor-mediated regulation.

DISCUSSION

TERE1/TBL2 PROTEIN INTERACTION AND LOCALIZATION

The TERE1/UBIAD1 protein has been previously reported to interact with APOE, an established mediator of cholesterol and triglyceride uptake and recycling and a vehicle for transport of vitamin K [McGarvey et al., 2005; Shearer and Newman, 2008]. In addition,

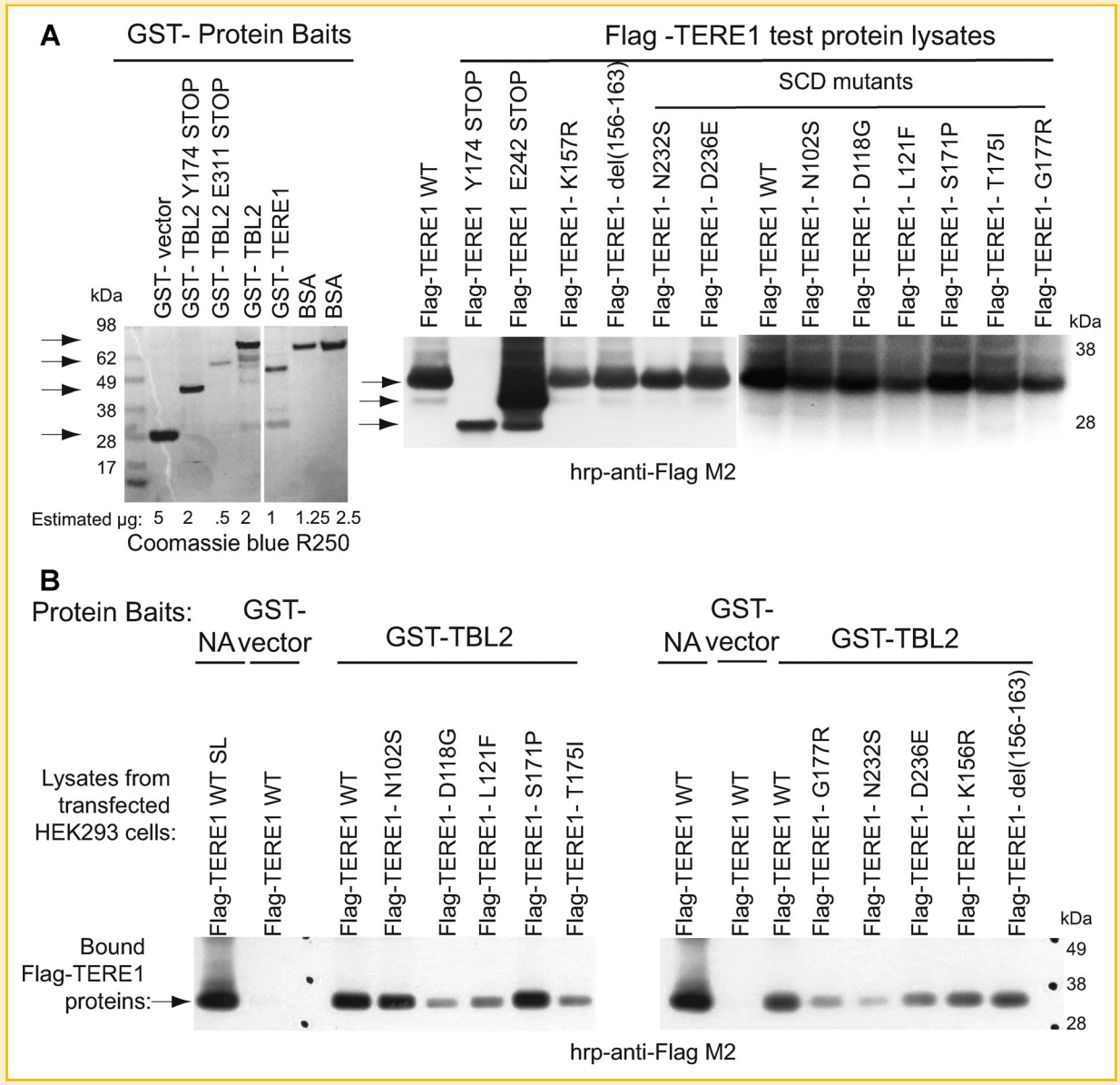

Fig. 6. Natural mutations in TERE1 associated with SCD affect binding to TBL2. (A) (Left panel) Coomassie blue R250 staining of GST fusion protein baits purified from bacteria and resolved via SDS–PAGE. (Right panel) Expression of Flag-TERE1 test proteins: wild type, deletions, and point mutants, in lysates of transfected HEK-293 cells after SDS–PAGE and hrp-anti-Flag-M2 immunoblotting. Similar expression levels are observed among different point mutant proteins that were tested for binding to purified GST-TBL2. B: Full length Flag-TERE1 wild type and point mutant protein cell lysates were ectopically expressed after transfection of HEK-293 cells. Reduced binding to full length GST-TBL2.is observed for TERE1 D118G, L121F, T175I, G177R, N232S, and D236E. SL refers to straight lysates. Binding was detected by immunoblotting with hrp-labeled anti-FLAG M2 antibody.

TERE1 was also found to interact directly with HMGcoA reductase, HMGR, a principal regulator of cholesterol synthesis, and SOAT-1, involved in cholesterol storage [Nickerson et al., 2013]. In this report we have validated the interaction of TERE1 with the TBL2 protein using a combination of two-hybrid assay, co-immunoprecipitation, GST-association, and co-localization to mitochondria. We found co-localization of endogenous TERE1 and TBL2 with the mitochondrial marker OXPHOS IV in J82 and T24 bladder cancer cells by immunofluoresence microscopy. TBL2 exhibited an exclusively peri-nuclear mitochondrial distribution. In addition to mitochondria, TERE1 also showed considerable non-mitochondrial localization. Given the caveat that standard immunofluoresence microscopy and biochemical subfractionation may not distinguish mitochondrial associated membranes MAMs which include ER: mitochondrial junctions from mitochondria [Lebiedzinska et al., 2009], we conducted immuno-electron microscopy to clarify the subcellular localization. Our immuno-electron microscopy of TERE1 and TBL2 confirms mitochondrial co-localization more definitively, and additionally confirms substantial non-mitochondrial TERE1.

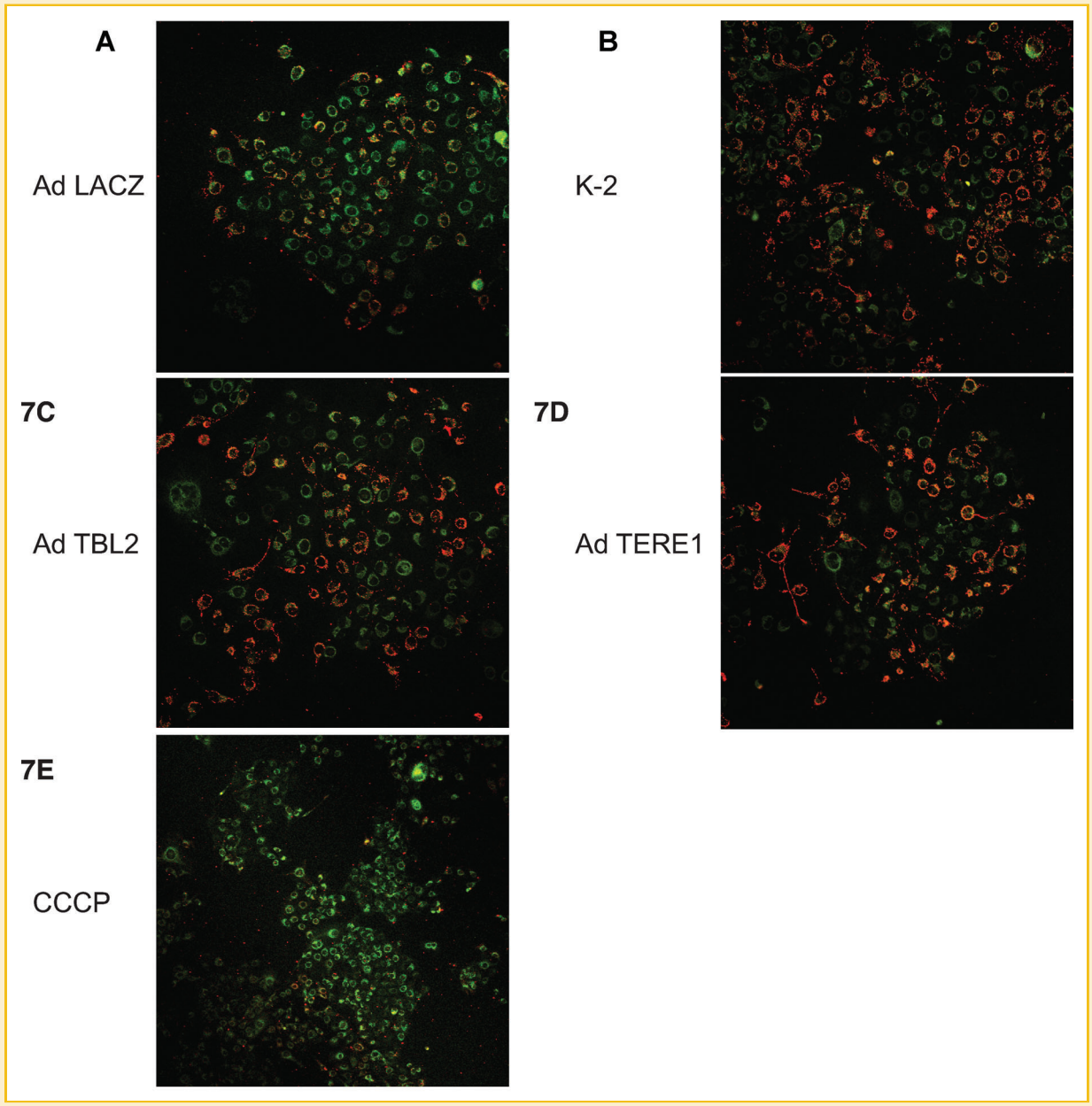

Fig. 7. Elevation of mitochondrial transmembrane potential by TERE1, TBL2, or K-2. J82 cells were treated for 72 h with Ad-LACZ, Ad-TERE1, or Ad-TBL2 or incubated for 1 h with vitamins K-2 or K-3 (30 μM). Confocal imaging was performed after loading cells with the voltage sensitive dye JC-1 (2 μM). As JC-1 accumulates and aggregates in mitochondria with increasing transmembrane potential, it undergoes a shift in emission from green to red. The mitochondrial uncoupler carbonyl cyanide m-chlorophenylhydrazone (CCCP; 50 nM), was used to confirm that the JC-1 response (green staining indicative of monomeric dye) was sensitive to membrane potential depolarization.

There is some variation in published reports on TERE1 function and subcellular localization in different biological systems. TERE1 was previously reported to co-immunoprecipitate with the mitochondrial matrix protein ATP5A from HEK-293 cells [Chanda et al., 2003]. A mitochondrial localization for TERE1(UBIAD1) was reported in human keratocytes [Nickerson et al., 2010]. TERE1 was also reported to localize to the ER in human osteoblast-like MG-63 cells and play a role in synthesis of menaquinone, vitamin K-2 [Nakagawa et al., 2010]. Recently, the Xenopus homolog of TERE1/UBIAD1, *barolo*, was found to localize to golgi and function in the synthesis of non-mitochondrial COQ10 in endothelial cells [Mugoni et al., 2013]. Overall, it is clear that the subcellular distribution of TERE1 (UBIAD1) differs in various cell types. Our previous immunohistochemical studies have found reduced TERE1 expression in invasive bladder cancer and metastatic prostate cancer specimens [McGarvey et al., 2001, 2003; Fredericks et al., 2011]. Whether the relative partitioning of TERE1 between ER, golgi, and mitochondria may be a dynamic mode of regulation that might vary in specialized cell

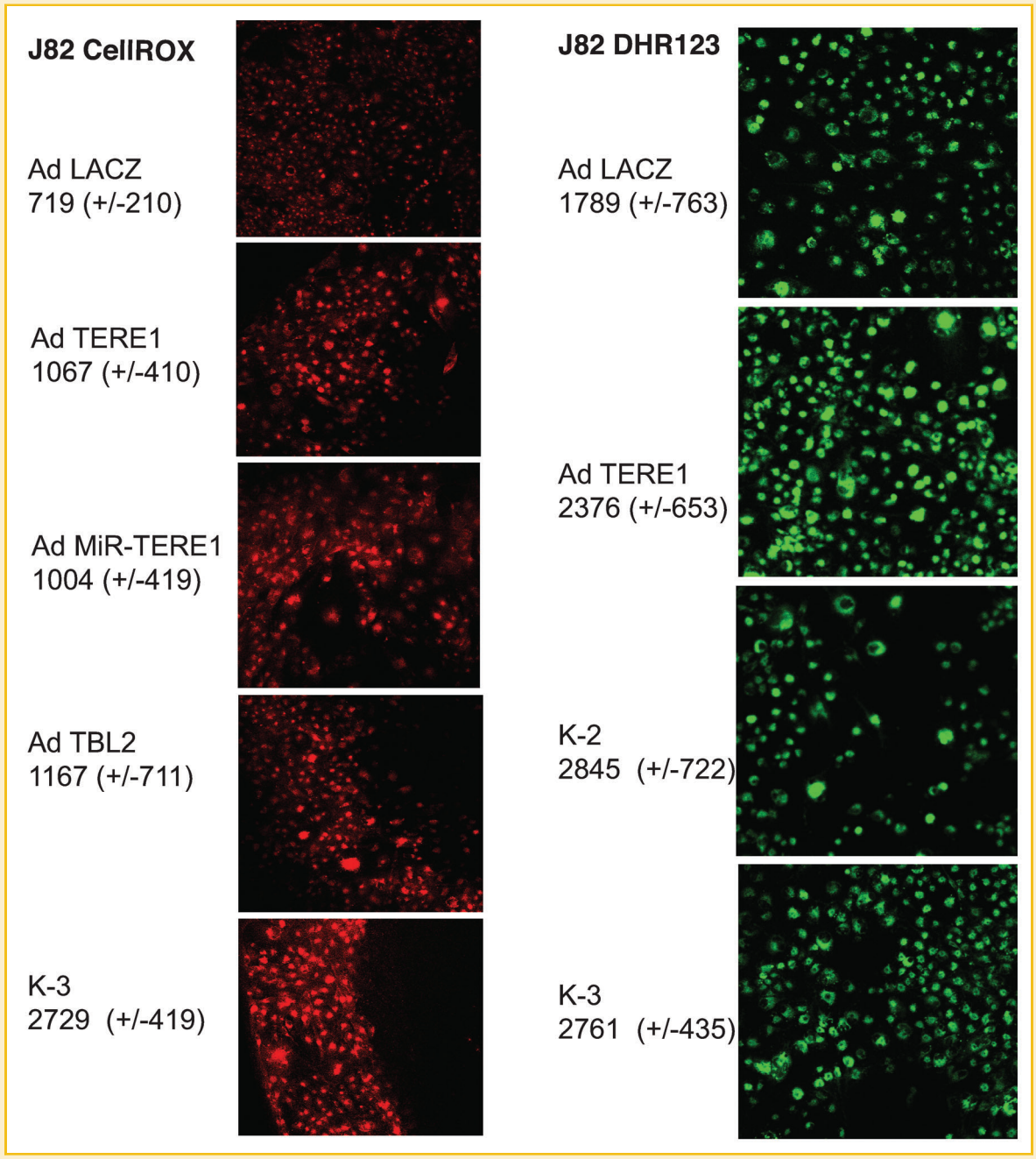

Fig. 8. Ectopic expression of TERE1, TBL2, or vitamins K-2 or K-3 elevate cellular ROS. J82 cells were treated for 60 h with Ad-LACZ, Ad-TERE1, or Ad-TBL2 or incubated for 1 h with vitamins K-2 or K-3 (30 μM). Confocal imaging was performed after loading cells with 5 μM of CellROX deep red or dihydrorhodamine 123 fluorogenic probes. Cellular fluorescence intensities were quantified after off-cell background subtraction.

types or be altered during tumor progression will require additional studies.

MITOCHONDRIAL TRANSMEMBRANE POTENTIAL, OXIDATIVE, AND NITROSATIVE STRESS

We found that ectopic TERE1 and TBL2 expression, as well as K-2 dosing, elevated the mitochondrial transmembrane potential in J82 cells. This is in agreement with menaquinone's capacity to facilitate electron transport in anaerobic states [Tielens et al., 2002; Nowicka and Kruk, 2010] and findings for the Drosophila homolog of TERE1, *heix*, in which expression enhanced mitochondrial electron transport and ATP production [Bhalerao and Clandinin, 2012; Vos et al., 2012]. Since the electron transport chain is an abundant source of mitochondrial superoxide radicals [Castello et al., 2006; Poyton et al., 2009; Cardoso et al., 2012], and menaquinone is known to undergo redox-cycling and generate reactive oxygen species

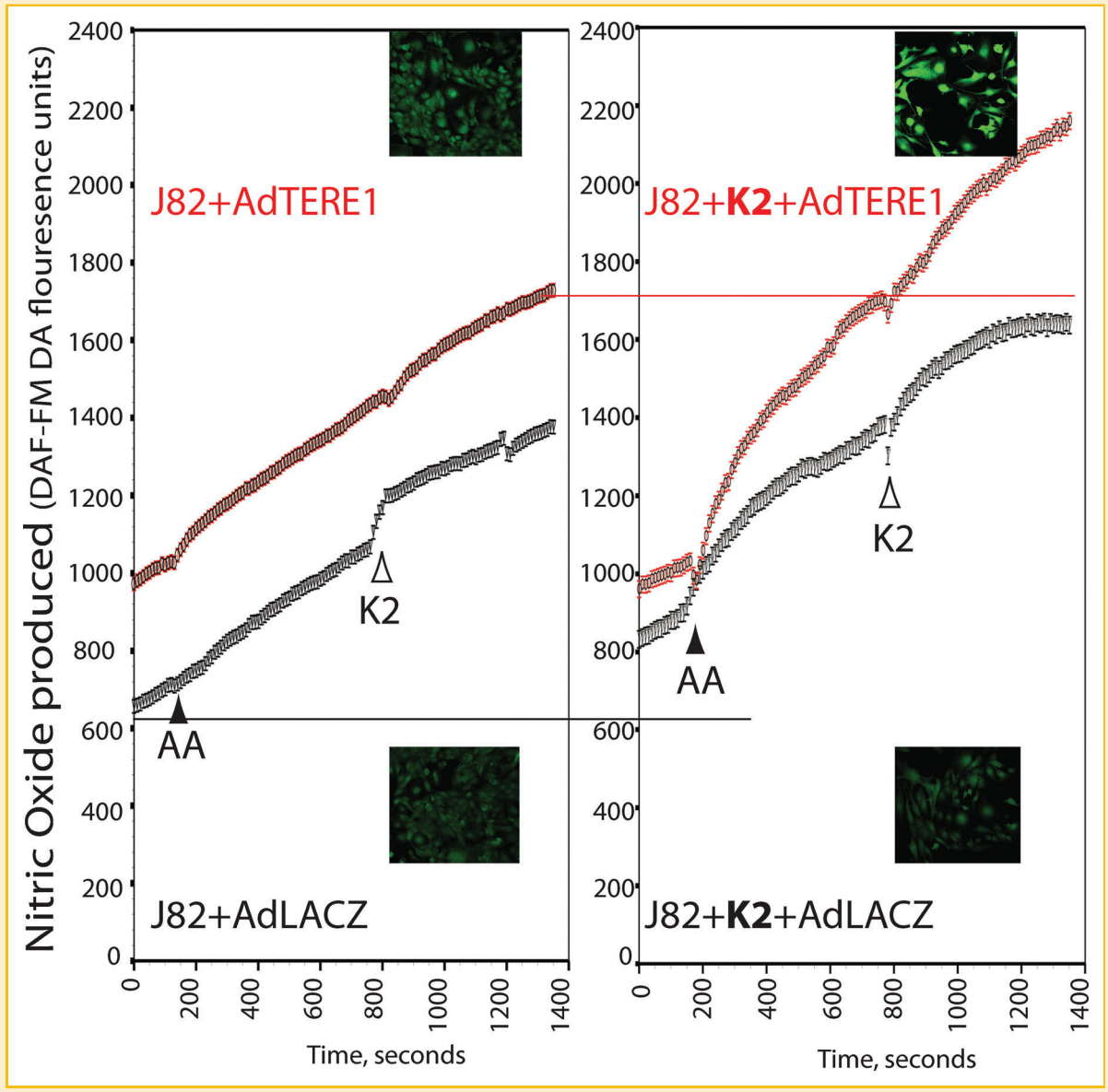

Fig. 9. Cellular NO/RNS production induced by ectopic TERE1 or vitamin K-2. Left panel, confocal imaging was performed on J82 cells that had been infected for 72 h with Ad-LACZ or Ad-TERE1 and loaded with DAF-FM-DA which reacts with NO and RNS to form a fluorescent benzotriazole. AA refers to minimal essential medium amino acids added to provide a source of arginine. K-2 refers to addition of vitamin K-2, menaquinone (30 μM). Images were captured at 10-s intervals. Right panel, the cells were pre-incubated with 30 μM K-2 for an hour prior to loading with DAF FM DA.

[Benz et al., 2006; Klaus et al., 2010], we conducted studies that demonstrate that ectopic TERE1 and TBL2 expression can affect the cellular levels of oxidative stress as evidenced by oxidation of the CellROX fluorogenic probe. We also found that ectopic TERE1 can increase caspase 3/7 activity two-fold. This shows that TERE1 expression can mimic some of the reported effects of pharmacological dosing of vitamins K-2 and K-3 that lead to different types of growth inhibition, autoschizis, necrosis, or apoptosis in different tumor cell lines [Lamson and Plaza, 2003; Shibayama-Imazu et al., 2008; Jamison et al., 2010]. TERE1 may be involved in phospho-activation of oxidative stress responsive signaling cascades as was previously shown for EGFR, ERK, ErbB2, and AKT in response to vitamin K-3 and attributed to inhibition of protein tyrosine phosphatases [Yoshikawa et al., 2007; Klaus et al., 2010]. Clearly many variables may influence the oxidative stress effects: TERE1 expression level and activity, substrate availability, subcellular location, prevailing oxygen tension, activity of cellular antioxidants, and reducing enzymes (refer to reviews [Nowicka and Kruk, 2010]). Others have reported that K-2 could induce iNOS [Sano et al., 1999], and that SXR activation could increase NO production [Verma et al., 2009]. Based on the ability of the mitochondrial respiratory chain to produce NO and other RNS [Castello et al., 2006; Poyton et al., 2009], we further determined that elevation of TERE1 expression increases the basal level of nitrosative stress as evidenced by NO production. The fact that

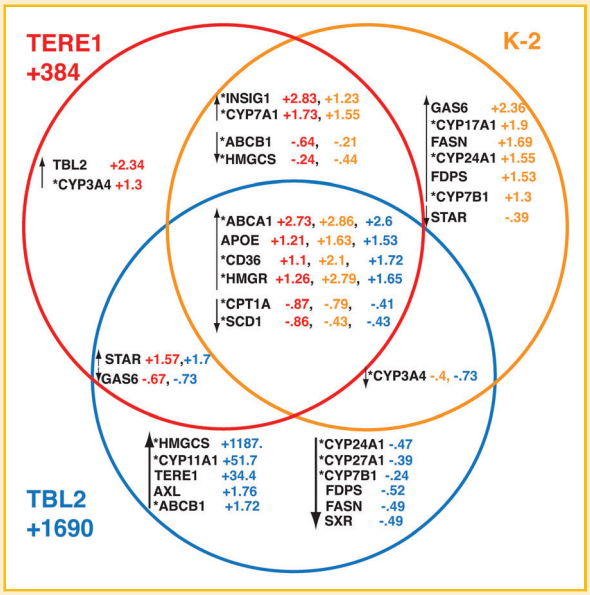

Fig. 10. TERE1, TBL2, and vitamin K-2 activate SXR target genes. The Venn diagram depicts the fold-change in expression of established SXR target genes (indicated by the asterisk*) by Fluidigm RT-PCR Taqman expression assays of J82 cells after three different induction treatments: TERE1 over-expression (red), vitamin K-2 30 μM overnight treatment (orange), and TBL2 over-expression (blue) relative to AD-LACZ or parental cell control and normalized as described in Materials and Methods Section. The data support the induction of changes in expression of known SXR target genes in cholesterol and fatty acid regulation.

exogenous K-2 could potentiate the rate of NO production within minutes implies direct chemical mechanisms play a role. Similar findings relating to NO production were recently reported concerning the Xenopus homolog of TERE1/UBIAD1, *barolo*, and were based on its proposed role in the synthesis of non-mitochondrial COQ10 which can regulate eNOS activity important for redox balance in endothelial cells [Mugoni et al., 2013]. Numerous studies implicate oxidative and nitrosative stress as driving forces in maintaining malignant progression associated with the invasive phenotype [Brown and Jessup, 2009; Ralph et al., 2010]. Our early observations that TERE1 level is reduced in invasive bladder and prostate cancer specimens suggests the possibility that TERE1 expression may be an oxidative stress liability that is selected against during tumor cell metabolic reprogramming to the invasive phenotype. We also measured an increase in ROS associated with TERE1 knockdown suggesting that TERE1 may function as an anti-oxidant and pro-oxidant depending on its level. Cells with lower levels of TERE1 may have a diminished capacity to sense oxidative stress and respond by triggering efflux, thus maintain an elevated oxidative stress. An additional possibility is that tumor cells with low levels of TERE1 and menaquinone are selected against in hypoxic anerobic environments and driven to invade.

MODULATION OF CHOLESTEROL AND SXR TARGET GENE EXPRESSION

We previously demonstrated that cellular cholesterol levels could be modulated by ectopic expression of TERE1 or TBL2 and suggested this was consistent with a mechanism of K-2 mediated SXR activation of cholesterol efflux [Shearer and Newman, 2008; Zhou et al., 2009b; Fredericks et al., 2011]. We have extended these results by showing that vitamin K-1, K-2, or K-3 can also reduce cellular cholesterol (Supplemental Fig. 6) and have supported this hypothesis by confirming that TERE1 and K-2, and TBL2 can activate expression of established SXR target genes. In the Venn diagram in Figure 10 there are six genes (ABCA1, CD36, HMGR, CPT1A, and SCD1) in the center that show common changes by each of the three induction treatments: (1) TERE1 overexpression, K-2 (30 μM), and TBL2 overexpression. Each of these genes is an established SXR target gene (indicated by the asterisk*) involved in lipid (ABCA1, HMGR) and fatty acid metabolism (CD36, CPT1A, and SCD1). Notably, ABCA1 is a major cholesterol efflux regulatory protein, thus its 2.73-, 2.86-, and 2.6-fold increase by each inducer, TERE1, K-2, and TBL2, respectively, would contribute to the reduction in cholesterol we have observed. APOE is an established LXR target gene, and a known TERE1-interacting protein [McGarvey et al., 2005; Fredericks et al., 2011]. (2) Considering SXR target genes commonly modulated by both TERE1 and K-2 are four with functions in cholesterol metabolism: INSIG1, CYP7A1, ABCB1, and HMGCS. CYP7A1 oxidizes cholesterol to 2-α-cholesterol for cellular export, hence increased CYP7A1 levels may facilitate export and contribute to the reduced cholesterol levels observed. INSIG1 elevation may inhibit SCAP-mediated transport of SREBP to golgi, hence prevent SREBP from activating cholesterol biosynthesis. INSIG1 can also bind HMGR resulting in its degradation, and further impair cholesterol synthesis. A decrease in HMGCS would also reduce cholesterol synthesis. Considering the TBL2 and TERE1 group, common changes include elevation of STAR, involved in cholesterol transport to mitochondria, and a slight reduction of GAS6, a ligand for AXL. (3) Finally there are expression changes unique to the individual induction treatments. TERE1 increased the SXR target, CYP3A4 and increased TBL2. It is interesting that elevation of TBL2 also increased TERE1. The reciprocal induction suggests a coordinated function. K-2 increased 3 SXR targets: CYP17A1, CYP24A1, and CYP7B1 involved in sterol metabolism, as well as the SREBP targets FASN and FDPS, involved in fatty acid and cholesterol synthesis, respectively. TBL2 strongly induced HMGCS involved in cholesterol synthesis, CYP11A1, involved in cholesterol side chain cleavage during conversion of cholesterol to pregnenolone in mitochondria, and ABCB1 encoding the P-glycoprotein efflux pump which can also efflux cholesterol. TBL2 decreased SXR targets: CYP24A1, CYP27A1, and CYP7B1 involved in vitamin D3 and cholesterol catabolism and FDPS and FASN involved in cholesterol and fatty acid synthesis.

Unlike the previously established relationship between vitamin K-2 and SXR activation, a mechanism explaining how TBL2 is involved in activation of SXR target genes is unclear, except by possible assistance of TERE1 mitochondrial function. TERE1 also interacts with APOE [Fredericks et al., 2011], and APOE is believed to play a role in oxysterol-induced efflux as part of a lipoprotein-mediated defense against oxidative stress [Rezen et al., 2010]. Thus, it is plausible that the role of TERE1 and TBL2 in activation of genes involved in cellular efflux may be a mechanism to relieve oxidative stress [Galea and Brown, 2009]. Overall these changes in expression of at least 15 SXR target genes support the hypothesis of SXR

activation by TERE1 and modulation of lipid homeostasis via cholesterol efflux and catabolism. This analysis will serve to guide further study of protein expression and signaling [Shearer and Newman, 2008; Verma et al., 2009; Zhou et al., 2009b].

COMMENTS ON TBL2

TBL2 is a WD repeat protein that our analysis has determined is a mitochondrial protein that interacts with TERE1. Like TERE1, ectopic TBL2 expression can increase mitochondrial transmembrane potential, elevate oxidative stress, reduce cholesterol levels, and activate several of the same SXR target genes involved in cellular efflux, and cholesterol and fatty acid metabolism. The mechanisms that govern TBL2 in these activities are undefined, however; by virtue of its inner mitochondrial membrane localization and association with TERE1, a role in metabolic redox signaling should be explored. This would be consistent with reports of TBL2 in a database of PDK1-binding proteins, suggesting a possible role in Thr 308 phospho-activation of AKT [Behrends et al., 2010]. It has also been shown that AKT activation by PDK1 is sensitive to redox, which may serve as a switch in decisions between proliferation or apoptosis [Antico Arciuch et al., 2009]. There are numerous studies evaluating the relationship between mitochondrial fission/fusion, oxidative stress, and mitophagy [Arduino et al., 2010; Lee et al., 2012]. The Drosophila UBIAD1/Heix protein was found to be a modifier of pink1, a gene mutated in Parkinson′s disease that affects mitochondrial function and regulates mitophagic turnover of mitochondria [Vos et al., 2012]. It is interesting to speculate that the WD repeats of TBL2, may be involved in similar functions as served by several other mitochondrial WD repeat proteins; namely, as scaffolds for protein complexes (MFN1, MFN2, Gβ2, OPA1, and Drp1) involved in mitochondrial fission/fusion [Tieu et al., 2002] and in responses to oxidative stress [Feng and Wang, 2012].

In summary, our findings support the idea that TERE1 has multiple modes of affecting cell function. First there are multiple subcellular locations: in non-mitochondrial membranous organelles such as ER, golgi, and others, and in mitochondria. There are direct chemical effects of K-2 on mitochondrial transmembrane potential, which lead to oxidative and nitrosative stress, affect cell redox status, and would initiate cell signaling. There are also effects of TERE1, TBL2, and K-2 that activate SXR target genes causing significant expression changes involved in lipid metabolism and cholesterol efflux. The loss of TERE1 expression in tumor cells may be a defect in mitochondrial to nuclear SXR signaling that tumors use to uncouple vitamin K-mediated oxidative stress sensing and signaling in mitochondria from apoptosis or negative growth signaling by elevation of cholesterol. Overall, these findings highlight the potential relevance of TERE1 expression in tumor cell bioenergetics, oxidative and nitrosative stress, and suggest a possible role for TERE1 in the adaptation to hypoxic microenvironments and invasiveness [Enns and Ladiges, 2012].

ACKNOWLEDGMENTS

We thank the Veterans Administration Merit Review and the Veterans Affairs Medical Center Philadelphia for the grant support to S.B. Malkowicz. We thank the Innisfree Foundation of Bryn Mawr, PA, and the Castleman Family Fund for their generous support to S.B. Malkowicz and W.J. Fredericks.

REFERENCES

Antico Arciuch VG, Galli S, Franco MC, Lam PY, Cadenas E, Carreras MC, Poderoso JJ. 2009. Akt1 intramitochondrial cycling is a crucial step in the redox modulation of cell cycle progression. PLoS ONE 4:e7523.

Arduino DM, Esteves AR, Oliveira CR, Cardoso SM. 2010. Mitochondrial metabolism modulation: A new therapeutic approach for Parkinson′s disease. CNS Neurol Disord Drug Targets 9:105–119.

Barrios-Rodiles M, Brown KR, Ozdamar B, Bose R, Liu Z, Donovan RS, Shinjo F, Liu Y, Dembowy J, Taylor IW, Luga V, Przulj N, Robinson M, Suzuki H, Hayashizaki Y, Jurisica I, Wrana JL. 2005. High-throughput mapping of a dynamic signaling network in mammalian cells. Science 307:1621–1625.

Behrends C, Sowa ME, Gygi SP, Harper JW. 2010. Network organization of the human autophagy system. Nature 466:68–76.

Benz CC, Atsriku C, Yau C, Britton D, Schilling B, Gibson BW, Baldwin MA, Scott GK. 2006. Novel pathways associated with quinone-induced stress in breast cancer cells. Drug Metab Rev 38:601–613.

Bhalerao S, Clandinin TR. 2012. Cell biology. Vitamin K2 takes charge. Science 336:1241–1242.

Brown AJ, Jessup W. 2009. Oxysterols: Sources, cellular storage and metabolism, and new insights into their roles in cholesterol homeostasis. Mol Aspects Med 30:111–122.

Cardoso AR, Chausse B, da Cunha FM, Luevano-Martinez LA, Marazzi TB, Pessoa PS, Queliconi BB, Kowaltowski AJ. 2012. Mitochondrial compartmentalization of redox processes. Free Radic Biol Med 52:2201–2208.

Castello PR, David PS, McClure T, Crook Z, Poyton RO. 2006. Mitochondrial cytochrome oxidase produces nitric oxide under hypoxic conditions: Implications for oxygen sensing and hypoxic signaling in eukaryotes. Cell Metab 3:277–287.

Chanda SK, White S, Orth AP, Reisdorph R, Miraglia L, Thomas RS, DeJesus P, Mason DE, Huang Q, Vega R, Yu DH, Nelson CG, Smith BM, Terry R, Linford AS, Yu Y, Chirn GW, Song C, Labow MA, Cohen D, King FJ, Peters EC, Schultz PG, Vogt PK, Hogenesch JB, Caldwell JS. 2003. Genome-scale functional profiling of the mammalian AP-1 signaling pathway. Proc Natl Acad Sci U S A 100:12153–12158.

Enns L, Ladiges W. 2012. Mitochondrial redox signaling and cancer invasiveness. J Bioenerg Biomembr 44:635–638.

Feng Y, Wang X. 2012. Antioxidant therapies for Alzheimer′s disease. Oxid Med Cell Longev 2012:472932.

Fredericks WJ, McGarvey T, Wang H, Lal P, Puthiyaveettil R, Tomaszewski J, Sepulveda J, Labelle E, Weiss JS, Nickerson ML, Kruth HS, Brandt W, Wessjohann LA, Malkowicz SB. 2011. The bladder tumor suppressor protein TERE1 (UBIAD1)modulates cell cholesterol: Implications for Tumor progression. DNA Cell Biol 11:851–864.

Galea AM, Brown AJ. 2009. Special relationship between sterols and oxygen: Were sterols an adaptation to aerobic life? Free Radic Biol Med 47:880–889.

Gilloteaux J, Jamison JM, Neal DR, Loukas M, Doberzstyn T, Summers JL. 2010. Cell damage and death by autoschizis in human bladder (RT4) carcinoma cells resulting from treatment with ascorbate and menadione. Ultrastruct Pathol 34:140–160.

Guda C, Subramaniam S. 2005. pTARGET [corrected] a new method for predicting protein subcellular localization in eukaryotes. Bioinformatics 21:3963–3969.

Ihunnah CA, Jiang M, Xie W. 2011. Nuclear receptor PXR, transcriptional circuits and metabolic relevance. Biochimica et Biophysica Acta (BBA): Bioenerg 1812:956–963.

Jamin N, Neumann JM, Ostuni MA, Vu TK, Yao ZX, Murail S, Robert JC, Giatzakis C, Papadopoulos V, Lacapere JJ. 2005. Characterization of the cholesterol recognition amino acid consensus sequence of the peripheral-type benzodiazepine receptor. Mol Endocrinol 19:588–594.

Jamison JM, Gilloteaux J, Perlaky L, Thiry M, Smetana K, Neal D, McGuire K, Summers JL. 2010. Nucleolar changes and fibrillarin redistribution following apatone treatment of human bladder carcinoma cells. J Histochem Cytochem 58:635–651.

Kathiresan S, Melander O, Guiducci C, Surti A, Burtt NP, Rieder MJ, Cooper GM, Roos C, Voight BF, Havulinna AS, Wahlstrand B, Hedner T, Corella D, Tai ES, Ordovas JM, Berglund G, Vartiainen E, Jousilahti P, Hedblad B, Taskinen MR, Newton-Cheh C, Salomaa V, Peltonen L, Groop L, Altshuler DM, Orho-Melander M. 2008. Six new loci associated with blood low-density lipoprotein cholesterol, high-density lipoprotein cholesterol or triglycerides in humans. Nat Genet 40:189–197.

Klaus V, Hartmann T, Gambini J, Graf P, Stahl W, Hartwig A, Klotz LO. 2010. 1,4-Naphthoquinones as inducers of oxidative damage and stress signaling in HaCaT human keratinocytes. Arch Biochem Biophys 496:93–100.

Lamson DW, Plaza SM. 2003. The anticancer effects of vitamin K. Altern Med Rev 8:303–318.

Lebiedzinska M, Szabadkai G, Jones AW, Duszynski J, Wieckowski MR. 2009. Interactions between the endoplasmic reticulum, mitochondria, plasma membrane and other subcellular organelles. Int J Biochem Cell Biol 41: 1805–1816.

Lee J, Giordano S, Zhang J. 2012. Autophagy, mitochondria and oxidative stress: Cross-talk and redox signalling. Biochem J 441:523–540.

Matsuoka S, Ballif BA, Smogorzewska A, McDonald ER, Hurov KE, Luo J, Bakalarski CE, Zhao Z, Solimini N, Lerenthal Y, Shiloh Y, Gygi SP, Elledge SJ. 2007. ATM and ATR substrate analysis reveals extensive protein networks responsive to DNA damage. Science 316:1160–1166.

McGarvey TW, Nguyen T, Tomaszewski JE, Monson FC, Malkowicz SB. 2001. Isolation and characterization of the TERE1 gene, a gene down-regulated in transitional cell carcinoma of the bladder. Oncogene 20:1042–1051.

McGarvey TW, Nguyen T, Puthiyaveettil R, Tomaszewski JE, Malkowicz SB. 2003. TERE1, a novel gene affecting growth regulation in prostate carcinoma. Prostate 54:144–155.

McGarvey TW, Nguyen TB, Malkowicz SB. 2005. An interaction between apolipoprotein E and TERE1 with a possible association with bladder tumor formation. J Cell Biochem 95:419–428.

Mugoni V, Postel R, Catanzaro V, De Luca E, Turco E, Digilio G, Silengo L, Murphy MP, Medana C, Stainier DY, Bakkers J, Santoro MM. 2013. Ubiad1 is an antioxidant enzyme that regulates eNOS activity by CoQ10 synthesis. Cell 152:504–518.

Nakagawa K, Hirota Y, Sawada N, Yuge N, Watanabe M, Uchino Y, Okuda N, Shimomura Y, Suhara Y, Okano T. 2010. Identification of UBIAD1 as a novel human menaquinone-4 biosynthetic enzyme. Nature 468:117–121.

Nickerson ML, Kostiha BN, Brandt W, Fredericks W, Xu KP, Yu FS, Gold B, Chodosh J, Goldberg M, Lu da W, Yamada M, Tervo TM, Grutzmacher R, Croasdale C, Hoeltzenbein M, Sutphin J, Malkowicz SB, Wessjohann L, Kruth HS, Dean M, Weiss JS. 2010. UBIAD1 mutation alters a mitochondrial prenyltransferase to cause Schnyder corneal dystrophy. PLoS ONE 5: e10760.

Nickerson ML, Bosley AD, Weiss JS, Kostiha BN, Hirota Y, Brandt W, Esposito D, Kinoshita S, Wessjohann L, Morham SG, Andresson T, Kruth HS, Okano T, Dean M. 2013. The UBIAD1 prenyltransferase links menaquione-4 synthesis to cholesterol metabolic enzymes. Hum Mutat 34:317–329.

Nishikawa Y, Wang Z, Kerns J, Wilcox CS, Carr BI. 1999. Inhibition of hepatoma cell growth in vitro by arylating and non-arylating K vitamin analogs. Significance of protein tyrosine phosphatase inhibition. J Biol Chem 274:34803–34810.

Nowicka B, Kruk J. 2010. Occurrence, biosynthesis and function of isoprenoid quinones. Biochim Biophys Acta 1797:1587–1605.

Perez Jurado LA, Wang YK, Francke U, Cruces J. 1999. TBL2, a novel transducin family member in the WBS deletion: Characterization of the complete sequence, genomic structure, transcriptional variants and the mouse ortholog. Cytogenet Cell Genet 86:277–284.

Poyton RO, Ball KA, Castello PR. 2009. Mitochondrial generation of free radicals and hypoxic signaling. Trends Endocrinol Metab 20:332–340.

Ralph SJ, Rodriguez-Enriquez S, Neuzil J, Saavedra E, Moreno-Sanchez R. 2010. The causes of cancer revisited: "Mitochondrial malignancy" and ROS-induced oncogenic transformation—Why mitochondria are targets for cancer therapy. Mol Aspects Med 31:145–170.

Rezen T, Rozman D, Pascussi JM, Monostory K. 2010. Interplay between cholesterol and drug metabolism. Biochim Biophys Acta 1814:146–160.

Sano M, Fujita H, Morita I, Uematsu H, Murota S. 1999. Vitamin K2 (menatetrenone) induces iNOS in bovine vascular smooth muscle cells: No relationship between nitric oxide production and gamma-carboxylation. J Nutr Sci Vitaminol (Tokyo) 45:711–723.

Shearer MJ, Newman P. 2008. Metabolism and cell biology of vitamin K. Thromb Haemost 100:530–547.

Shibayama-Imazu T, Aiuchi T, Nakaya K. 2008. Vitamin K2-mediated apoptosis in cancer cells: Role of mitochondrial transmembrane potential. Vitam Horm 78:211–226.

Spurgeon SL, Jones RC, Ramakrishnan R. 2008. High throughput gene expression measurement with real time PCR in a microfluidic dynamic array. PLoS ONE 3:e1662.

Tielens AG, Rotte C, van Hellemond JJ, Martin W. 2002. Mitochondria as we don′t know them. Trends Biochem Sci 27:564–572.

Tieu Q, Okreglak V, Naylor K, Nunnari J. 2002. The WD repeat protein, Mdv1p, functions as a molecular adaptor by interacting with Dnm1p and Fis1p during mitochondrial fission. J Cell Biol 158:445–452.

Verma S, Tabb MM, Blumberg B. 2009. Activation of the steroid and xenobiotic receptor, SXR, induces apoptosis in breast cancer cells. BMC Cancer 9:3.

Vos M, Esposito G, Edirisinghe JN, Vilain S, Haddad DM, Slabbaert JR, Van Meensel S, Schaap O, De Strooper B, Meganathan R, Morais VA, Verstreken P. 2012. Vitamin K2 is a mitochondrial electron carrier that rescues pink1 deficiency. Science 336:1306–1310.

Weiss JS, Kruth HS, Kuivaniemi H, Tromp G, White PS, Winters RS, Lisch W, Henn W, Denninger E, Krause M, Wasson P, Ebenezer N, Mahurkar S, Nickerson ML. 2007. Mutations in the UBIAD1 gene on chromosome short arm 1, region 36, cause Schnyder crystalline corneal dystrophy. Invest Ophthalmol Vis Sci 48:5007–5012.

Yoshikawa K, Nigorikawa K, Tsukamoto M, Tamura N, Hazeki K, Hazeki O. 2007. Inhibition of PTEN and activation of Akt by menadione. Biochim Biophys Acta 1770:687–693.

Zhou C, King N, Chen KY, Breslow JL. 2009a. Activation of PXR induces hypercholesterolemia in wild-type and accelerates atherosclerosis in apoE deficient mice. J Lipid Res 50:2004–2013.

Zhou C, Verma S, Blumberg B. 2009b. The steroid and xenobiotic receptor (SXR), beyond xenobiotic metabolism. Nucl Recept Signal 7:e001.

SUPPORTING INFORMATION

Additional supporting information may be found in the online version of this article at the publisher's web-site.

Fig. S1. Endogenous TERE1 and TBL2 expression in the J82 transitional cell carcinoma cell line after extraction of sub-cellular fractions. Equal amounts of protein were analyzed by immunoblots with 1A. Top: Goat anti-TERE1 (NH2), and, 1B. Bottom: rabbit anti-TBL2 (216–309) or Ch-anti TBL2 (353–366). The left panels show

TERE1 (top) and TBL2 (bottom) are enriched in membranous/organellar fractions. Exogenous FLAG-tagged-TERE1 and -TBL2 serve as positive controls. Right panels: Immunoblot detection of TERE1 and TBL2 in an isolated human liver mitochondrial subcellular fraction obtained from MitoScience, Inc., and from whole cell lysates of HEK-293 cells transfected with TERE and TBL2.

Fig. S2. Immunoflourescent detection of TERE1 and TBL2 in J82 and T24 bladder cancer cell lines with a panel of polyclonal antibodies. Antibodies were affinity purified against peptide antigens and cells were prepared and images collected as described in Materials and Methods Section. A similar peri-nuclear/organellar, mitochondrial pattern was observed for all the TERE1 antibodies and the rabbit anti-TBL2 (111–129) antibody.

Fig. S3. Deletion analysis of TERE1 and TBL2 interaction. The NH2 terminal third of TBL2 is sufficient for binding to the middle third of TERE1. 3A. Flag-TERE1 test proteins (full length 339 and deletions, E242 STOP, and Y174 STOP) were tested for binding to GST-TBL2 bait proteins (full length 449 and deletions E311 STOP and Y174 STOP). 3B. Reverse configuration. Flag-TBL2 test proteins (full length and deletions, E311 STOP and Y174 STOP) were tested for binding to GST-TERE1 bait proteins (full length and deletions, E242 STOP, and Y174 STOP). Binding was detected with hrp-anti-FLAG M2 secondary antibody.

Fig. S4. FLAG-TERE1 and -SMURF1 bind to GST-TBL2 bait. Bound FLAG proteins were resolved by SDS–PAGE and were detected on immunoblots probed with hrp-anti-FLAG antibody.

Fig. S5. Ectopic TERE1 increases J82 cell caspase 3/7 activity. J82 cells were infected with Ad-LACZ, Ad-TERE1 or Ad-MiRNA TERE1. Assays were conducted in 96-well luminometry plates using the Caspase-Glo 3/7 kit from Promega after 60 h.

Fig. S6. Vitamin K treatments or ectopic TERE1 and TBL2 expression result in cholesterol reduction. 6A. Treatment of J82 cells with vitamin K-1 (30 μM), K-2 (30 μM), or K-3 (10 μM) or ectopic expression of TERE1 and TBL2 proteins for 72 h results in a reduced level of cellular cholesterol compared to untreated or Ad-LACZ Vector control. Cell lysates were analyzed by Amplex Red assay for cholesterol and by BCA for protein.

Table SI. Two-Hybrid Assay of TERE1 and TBL2 Interaction. The *Test Interaction Between TERE1 and TBL2 is Detected by the Presence of Colonies Under 3-AT Selective Conditions